QATAR UNIVERSITY

COLLEGE OF ARTS AND SCIENCE

SYNTHESIS AND PROPERTIES OF NANOCRYSTALLINE BI-TE

BASED THERMOELECTRIC MATERIALS FOR ENERGY

APPLICATION

BY

MANAL ALSALAMA

A thesis submitted to the Faculty of

College of Arts and Sciences

In Partial Fulfillment of the Requirements for the Degree of

Master of Science

Materials Science and technology

June 2016

COMMITITEE PAGE

The members of the committee approve the thesis of Manal Alsalama

defended in 26th of May, 2016.

                    _____

                              Khaled Youssef

                          Thesis supervisor

                    _____

                               Ahmed Abdala

                          Committee member

                    _____

                               Ahmad Ayesh

                          Committee member

Approved:

_____

Eiman Mustafawi, Dean, College of Arts and Sciences

ABSTRACT

Thermoelectric phenomenon is the science associated with converting thermal energy into electricity based on the Seebeck effect. Bismuth telluride Bi_2Te_3 is currently considered to be the state-of-the art thermoelectric material with high efficiency for low temperature applications and is therefore attractive for energy harvesting processes. Nanostructures thermoelectric materials provide a novel way to enhance thermoelectric properties and are considered to be the efficient building blocks for thermoelectric devices. In this work, n- and p-type bulk nanocrystalline Bismuth telluride thermoelectric materials were prepared by mechanical alloying / ball milling technique. The produced nano-crystalline powder were then consolidated using hot compaction under inert atmosphere. The novel processing of these materials maintained the nanostructure in both n- and p-type. Structural properties of the n- and p-types were characterized using X ray diffraction, scanning electron microscopy and transmission electron microscope. These techniques proved that the average grian size of the milled thermoelectric materials was about 20 nm. Accordingly, a Significant improvement in the figure of merit (ZT) is achieved through significant lattice thermal conductivity reduction and Seebeck coefficient improvement. The maximum ZT value for the n-type nanocrystalline thermoelectric was 1.67 at 373 K while the maximum ZT value for the p-type was 1.78 at the same temperature. These values are considered to be the highest values reported for similar materials. Evaluation of the mechanical properties was also performed through microhardness measurement using Vickers micro-hardness test, which shows an enhancement in mechanical properties for the produced materials.

Table of Contents

List of Tables

List of Figures

Acknowledgement

All praise and thanks be to Allah first and foremost then to all people, whom without their corporation, patience and support, this work would have never been in its final form. First, I would like to express my highly appreciation to my supervisor Dr. Khaled Youssef, for giving me the chance to work under his supervision and for his great academic guiding and continuous support.

I would like also to thank the rest of my thesis committee: Dr. Ahmad Ayesh and Dr. Ahmed Abdulla for their encouragement and insightful comments and advices.

Appreciation goes to Central of Advanced Materials and Central Lab unit for their assistance in the experimental work.

I am deeply grateful to my brother, Dr. Haitham for his continuous guidance and giving me his precious time and advice whenever I needed it. Without him I would not be where I am today.

My heartfelt appreciation goes to my brother, Ahmad for his continuous technological support and valuable advices.

Special thanks to my friends Sara and Nour for their continuous support in the long way of master studying.

Dedication

This work is lovingly dedicated to;

My role model, my father who taught me "where there is a well, there is a way",

My mother for her great efforts and support,

My husband for his patience, support and encouragement,

All my brothers and sisters,

The noble woman, who taught me the great value of hard work, my doctor, Laila Babsail.

To my four little angels, my kids, who give me wonderful love and support. Their love,

hugs and jokes had cheered me up all those years.

CHAPTER 1

INTRODUCTION

The demand of energy is increasing continuously in all over the world in conjunction of facing the problems of global warming and dropping of oil and gas levels. These concerns have led to a huge focus on renewable and green energy sources as good alternatives for fossil fuels. It is worth mentioning that large amount of these fuels are not used and lost in the form of wasted heat. large amount of wasted heat is produced from automobiles and industrial operations because of fuel consumption. If part of this heat can be successfully reused to produce electrical energy, this would be an excellent way to reduce greenhouse emission and pollution and would be an effective solution for energy demand [1]. Thermoelectric is a powerful promising technique that is used to convert heat into useful power. The conversion efficiency plays an important role in the current challenges for developing alternative energy technologies to reduce the use of fossil fuels. Thermoelectric materials attract the attention of researchers because of their ability to convert directly and reversibly heat to electrical energy. The attractive features of thermoelectric devices are their long life, low maintenance, high reliability, no moving part included, light weight as well as they do not produce emissions harmful to the environment. Thermoelectric generators are used to provide electrical power in medical, military, and space applications where their desirable properties outweigh their relatively high cost and low operating efficiency [1], [2]. The idea of thermoelectric effect has been

used for century ago, the first use of thermoelectric materials was by silicon germanium alloys at high temperature for space application [3]. However, widespread use of thermoelectric components is presently limited by the low values of figure-of-merit for presently known materials and low efficiency. Since 1990's, a significant progress is done in the field of thermoelectrics. Nano-structuring was found experimentally as an effective way for enhancing thermoelectric materials efficiency by enhancing figure of merit [4]. Figure of merit is defined as $ZT = S^2 \sigma / K_{tot}$, where S, σ and K_{tot} are Seebeck coefficient, electrical conductivity and total thermal conductivity, respectively [2]. Nanostructure materials means producing grains and phases that have at least one dimension in nanoscale. Reducing the size of the material results in high density of boundaries that act as barrier to scatter phonons and to scatter low charge carriers, hence help in reducing lattice thermal conductivity and enhancing Seebeck coefficient [5]. Several work has been done in this field using several preparation methods like vapor deposition, chemical methods, melt spinning. The highest ZT of 2.4 was achieved in super lattices thermoelectric materials that prepared by vapor deposition [6]. However, the produced materials could not be used practically in industry. High cost of fabrication, difficulty of scaling up the materials to devices, limited amount of produced materials are all challenges faced in the field of producing thermoelectric devices [7]. Powder metallurgy technique which is Mechanical alloying / ball milling was found to be an effective preparation technique that is able to overcome most of the disadvantages of other preparation techniques. It has the advantages of low cost, easy handling, and been environmentally friendly [8]. It is used accompanied with compaction techniques to

14

consolidate the material into bulk that could be used for fabrication of thermoelectric devices [9]. Further details about effective thermoelectric materials are provided in chapter 2.

Bismuth telluride with its alloys have been the most material used at low temperature for thermoelectric applications. However, it has low ZT value (close to1) compared to traditional electrical generators. ZT value of 3 or more is needed for thermoelectric materials to compete with the traditional electrical generators. However, many work was done on Bismuth telluride materials to enhance their thermoelectric properties such as doping and nano-structuring [10].

The focus of this work is to overcome the challenges of enhancing ZT of Bi-Te through reducing grain size. We have successfully produced nano-bulk n-and p-type bismuth telluride materials using mechanical alloying technique followed by hot compaction. The materials are produced from elemental powders which help in conserving energy that could be consumed during milling of large particles or used to produce the material ingots. Optimum conditions were used for hot compaction that help in keeping the final products in the nano-scale. The structural characterization of both samples were done by XRD, SEM and TEM. The thermal behavior was studied by differential scanning calorimeter and mechanical properties (hardness) was measured using micro-hardness test. Thermoelectric properties were determined using single measurement run based on the system proposed by Schwyer et al. The results show an improvement in thermoelectric properties compared to state-of- the art materials. We have obtained high

ZT for p- and n- type of 1.78 and 1.688, respectively, which are the highest figure of merit reported to our knowledge among all nanobulk bismuth telluride materials. Through the experimental part, the preparation, the characterization methods and the results are discussed in chapter 3, 4 and 5.

CHAPTER 2

LITERATURE REVIEW

2.1 Thermoelectric properties

Thermoelectric effect can be easily defined as a phenomenon where temperature difference is directly converted into electric voltage and vice versa. Thermoelectric effect includes three identified phenomena, Seebeck effect, Peltier effect and Thomson effect. Thermoelectric devices act as thermoelectric generators if they generate electricity when subjected to a temperature difference on both sides. Conversely they act as refrigerators and pump heat when current pass through them. Improving thermoelectric properties is the key challenge to obtain high efficient thermoelectric materials. Good thermoelectric materials should have high electrical properties and low thermal conductivity. These aspects are combined in a property called figure of merit. Enhancing figure of merit is the main issue in the field of thermoelectrics [11]. Thermoelectric properties will be discussed in details in the next few sections.

2.1.1 Figure of merit

The efficiency of thermoelectric materials is determined their ability to convert efficiency and the maximum value of efficiency is determined by Carnot efficiency. However, it depends strongly on a property of the material, figure of merit, ZT. The concept of figure

of merit was first introduced by Altenkrich in 1911 to help predicting the best conditions of thermoelectric conversion. Z is calculated [12] by the following relation

$$Z = \frac{S^2 \, \sigma}{K_{tot}} \qquad (2.1)$$

As can be concluded from equation (2.1), Z is a function to three physical properties of the material; Seebeck coefficient (S), electrical conductivity (σ) and thermal conductivity K_{tot}. K_{tot} represents a contribution from K_e (the heat transferred by electrons) and K_l (heat transferred by lattice phonons). Thus, it is suitable to write K as the sum of both contributions ($K_{tot} = K_e + K_l$). The term ($S^2 \, \sigma$) is called power factor and represents the material's electronic properties part [12]–[14]. It should be taken into account the dependency of the three properties on temperature so it is better to multiply both sides of the equation by T to get a dimensionless figure of merit ZT, where T is the average temperature that all the properties are measured at. So relation (2.1) could be rewritten as [2], [15]

$$ZT = \frac{S^2 \, \sigma}{K_{tot}} T \qquad (2.2)$$

In order to improve thermoelectric performance, ZT must be increased. High ZT implies high values of both Seebeck coefficient and electrical conductivity with low value of thermal conductivity. Materials with high figure of merit have high conversion efficiency and considered as effective thermoelectric materials. Early work on thermoelectrics was on metals, which possess very small values of ZT (lower than unity). Good progress has

been done and nowadays ZT starting to get higher than 1 at room temperature for traditional thermoelectric materials such as bismuth telluride and lead telluride. The highest ZT value of 2.4 was achieved for super lattices, which is basically a result of thermal conductivity reduction [6]. Although materials with ZT equals to 1 are considered useful, current refrigeration technology cannot be replaced unless ZT reach a value of 3 or more [16], [17].

2.1.2 Seebeck, Peltier and Thomson effect

The basic concept behind thermoelectric behavior based on Seebeck and Peltier effects. These effects occur because charge carriers transport heat as well as electricity. The relationship between these two effects is a third effect defined by Thomson effect [18]. The main concepts will be briefly explained in the following sections.

Seebeck effect

Seebeck effect was discovered in 1821 by Johan Seebeck. He noticed the deflection of a compass needle that was placed close to a cycle of two joint dissimilar materials subjected to temperature gradient. This refers to a magnetic field that should necessarily require the presence of an electric potential. The voltage difference produced is directly proportional to the temperature gradient at the two ends of the material. This could be understood by considering a rod of metal heated from one side and cooled at the other end. The charge carriers tend to move from the hot side of the material to the cold one and establish a potential difference as shown in Figure 2.1. [18], [19].

Figure 2.1: Charge transportation from hot end to the cold end [1]

The relationship between the temperature difference ΔT and the resulting voltage difference ΔV is given by

$$\Delta V = S \Delta T \tag{2.3}$$

Where S is the Seebeck coefficient, a constant related to the intrinsic property of the material. Metals for example have low values of Seebeck coefficient (less than some tens of microvolts per degree) while it is much higher for semiconductors (1-2 millivolts per degree) [18].

Peltier effect

Peltier effect was discovered by scientist Peltier in 1834. This effect is figured when the current flow through the material results in heat absorption at the cold side and rejection at the hot side. Peltier effect mainly measures the amount of heat carried by charge carriers. It is related to the electric current by the following relation: [2][20] [8]

$$\Pi = \frac{Q}{I} \tag{2.4}$$

Where Π is the Peltier coefficient, Q is amount of heat carried by charge carriers and I is the electric current.

Devices that are controlled by Seebeck effect are thermoelectric generators (TEG), while ones controlled by Peltier effect are thermoelectric coolers (TEC). Figure 2.2 illustrates the generation and cooler mode of thermoelectric materials.
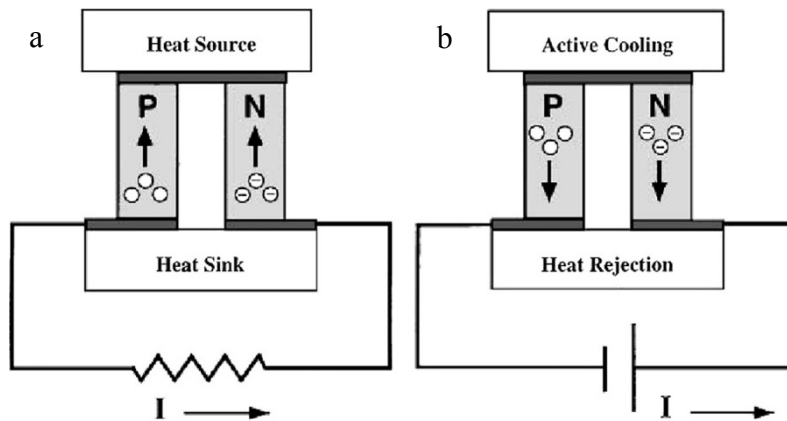
Figure 2.2. a) generation mode b) cooling mode of thermoelectric materials [16]

Thomson effect

When both Seebeck and Peltier effects are presented in a single material and the current flow through the sample at the same time is subjected to temperature gradient, the effect then called Thomson effect. This effect was established in 1855 by Kelvin (who was known as William Thomson) and it consists of reversible heating or cooling process.

Heat will be rejected if the current flows in the same direction of the heat flow or it will be absorbed along the sample if the current is in the opposite direction to the heat flow. Thomson found two relationships; the first between Seebeck (S) and Peltier (Π) coefficient where [21].

$$\Pi = ST \tag{2.5}$$

T is the absolute temperature.

The second is the relation between the rate of heating per unit length ($\frac{dQ}{dX}$), the temperature gradient ($\frac{dT}{dX}$) and the electric current:

$$\frac{dQ}{dX} = \tau\, I\, \frac{dT}{dX} \tag{2.6}$$

Where (τ) is Thomas coefficient [21].

2.1.3 Electrical transport in thermoelectric materials

The electrical transport properties included Seebeck coefficient, electrical resistivity and electrical mobility. Electrical transport properties are determined by the structure of the material, the material temperature and several charge carriers scattering processes [1], [11]. Each of these properties will be discussed in more details in the following sections.

2.1.3.1 Seebeck coefficient

Seebeck coefficient measures the magnitude of thermoelectric voltage as a result of temperature difference and describes the interaction between thermal and an electrical current across thermoelectric material. It is expressed in unit of $\mu V/K$ and has two contributions; charge carriers diffusion (S_d) and phonon drag (S_g). Thus $S = S_d + S_g$ [22].

Diffusive Seebeck coefficient

This part of Seebeck coefficient arises from the difference in the diffusion rate of charge carriers according to a temperature gradient. As in classical gases where molecules expand when heated, charge carriers diffuse from the hot side to the cold one when the material is subjected to a temperature difference. They leave an opposite charged behind them, resulting in building potential difference between the two ends. This separation of charges gives rise to an electric potential, which will limit the buildup of charges at the cold end. Thus, some of the charge carriers will drift back to the hot side in the direction of the electric field. These two processes of charge carriers drifting in opposite direction are competing. No net current will be produced unless one of the processes is stronger than the other. Therefore, heavily doped semiconductors with an excess amount of one charge type are suitable for enhancing the value of Seebeck coefficient. The sign of Seebeck coefficient in doped semiconductors depends on the sign of the excess charge carriers. So it is positive in the case of holes and negative in the case of electrons [22].

Temperature is not the only factor that determines the diffusion rate of charge carriers. Impurities and imperfections contribute in the carriers scattering. If the scattering depends on the energy of carriers, hot and cold carriers will diffuse with different rates, therefore creating a higher density of one type of charge carrier at one end of the material [22].

Phonon drag Seebeck coefficient

In solids, charge carriers are not alone but they are surrounding by vibrating atoms. Thus phonons affect the transporting properties. Although phonons do not carry electric charges, they can disturb the movement of them by scattering. This part of Seebeck coefficient attributed to the generation of phonon current transporting heat. During the movement, they interact and drag their momentum to the charge carriers and sweep them to one end of the material. Phonon drag component varies with temperature. It mostly vanishes at room temperature and above for most solids. However, it is predominant at lower temperature where [22]

$$T \approx \frac{\theta_D}{5} \tag{2.7}$$

θ_D is Debye temperature, the temperature that causes the excitement of high frequency phonons. Phonon drag component is also affected by charge carrier concentration and inversely proportional to it by the following relation

$$S_g = -\frac{1}{3}\frac{C_l}{ne} \tag{2.8}$$

Where C_l is the lattice specific heat, n is the concentration of charge carriers and e is the electric charge. Thus for heavily doped semiconductors and at high temperature (above room temperature), the contribution of phonon drag in Seebeck coefficient is negligible [11], [23], [24].

2.1.3.2 Electrical resistivity and mobility

Electrical resistivity is an important intrinsic property of the material, which describes how strong the material opposes the motion of the charge carriers. Its value is a function of temperature and an indicative of the type of material. For semiconductors, the value of resistivity is determined by two factors; carrier concentration and carriers' mobility (mean free path) [12].

$$\rho = 1/q \ (\mu_n \ n + \mu_p \ p) \tag{2.9}$$

Where μ_p and μ_n are holes and electrons mobility, respectively. n and p are the electrons and holes concentration, respectively. For heavily doped semiconductors equation (2.9) can be reduced to a single term since the concentration of majority carriers are much higher than minority carriers. The mobility of charge carriers is affected by temperature and the scattering mechanism. The scattering could be due to lattice vibration, impurities and defects. As the temperature increases, lattice vibration increases thus resistivity increases. Furthermore, the presence of defects and impurities will cause more scattering of charge carriers and hence high resistivity [12]. The effect of temperature and scattering

process on increasing the value of resistivity was reported for many thermoelectric materials [25], [26].

2.1.4 Thermal transport in thermoelectric materials

In solid materials, heat could be transferred by charge carriers as well as by lattice waves (phonons). Thus, thermal conductivity in thermoelectric materials consists of two components; electric (K_e) and lattice (K_l). Thermal conductivity is defined as [27]

$$K = -\frac{Q}{\Delta T} \tag{2.10}$$

Thus, it is the heat flow rate per unit area in a direction normal to the surface of this area (Q) per unit of temperature gradient (ΔT). Thermal conductivity differs from one material to another and its value is affected by several factors including; lattice defects, the interaction between lattice phonons and charge carriers, the grain size in polycrystalline material and the sample size in single crystal [27].

2.1.4.1 Electronic Thermal conductivity

Charge carriers conduct electricity as well as heat. Thus, there is a relation between electronic thermal conductivity (K_e) and electrical conductivity (σ). This relation is given by Windeman-Franz law [11]

$$K_e = L\,\sigma\,T \tag{2.11}$$

Where L is the Lorenz number varies between 1.5 for non- degenerated semiconductors and $2.44 \times 10^{-8}\,W\Omega\,K^{-2}$ for strongly degenerated ones, T is the absolute temperature. When a wide range of temperature is considered including low temperatures (lower than room temperature) one more element of heat transport should be added to the electronic thermal conductivity, which is bipolar diffusion term. K_{bi} arises from the recombination process of electron- hole pairs at the cold side after creation of them at hot side. In non-degenerated systems (like case of intrinsic semiconductors) where both electrons and holes have the same concentration and mobility, K_{bi} has a noticeable value while in degenerated systems (like the case of doped semiconductors) where only one carrier type has high mobility, it depends on the mobility of the minority carriers. As in thermoelectric field, the focus is on the degenerated systems, bipolar contribution could be suppressed by reducing the transport of minority carriers. Several aspects such as reducing the effective mass of the minority carriers, increasing their scattering or increasing the band gap can help in reducing the transport of minority carriers. For good thermoelectric materials, thermal conductivity should be as minimum as possible. However, decreasing the electronic part of thermal conductivity will result in decreasing the electrical conductivity of the material. Thus, optimizing ZT is done to reduce the lattice part of thermal conductivity while maintaining the electronic part [12], [28].

2.1.4.2 Lattice thermal conductivity

In non-metals materials, the main and dominant contribution to thermal conductivity is the lattice thermal conductivity which is due to lattice vibration (phonon motion) [11],

[27]. The lowest value of thermal conductivity is found in amorphous materials like glass where the heat is randomly moved through the lattice rather than rapid phonon transport. Lattice thermal conductivity is determined mainly by the phonons mean free path. The relationship between lattice thermal conductivity (K_l) and mean free path (l) is given by

$$K_l = \frac{1}{3} C_v \, v \, l \tag{2.12}$$

Where C_v is the heat capacity and v is the velocity of sound. The phonon mean free path (which is the path that phonon could walk before scattering) range from 1 nm to more than 10 μm. The minimum thermal conductivity was defined by Slack to be limited by interatomic distances in the crystal. Thus, there is a need to produce scattering agents, which are comparable to mean free path values in order to increase scattering of phonons and reducing lattice thermal conductivity. Thus, thermoelectrics require materials with phonon glass behavior to reduce lattice thermal conductivity and electron crystal behavior to keep good electrical conductivity [18], [28].

2.2 Challenges and ways for enhancing figure of merit

The main challenge in the topic of high efficient thermoelectric materials is to have materials with high ZT. From relation (2.1), one can think that it is as easy as to increase Seebeck coefficient and electrical conductivity and decrease thermal conductivity. However, it is not easy and it is much more complicated. All the properties are interrelated and laws of physics conspire against achieving these condition at the same time. The reason is that materials like metals, which have good electrical properties, have

good thermal properties as well. Insulators such as glass insulate electricity as well as heat. Thermoelectric properties are functions of several common factors like carrier concentration and effective mass but they are oppositely proportional to them. Electrical conductivity (σ) for example is related to the carrier concentration by the following relation

$$\sigma = n\,e\,\mu_e + p\,e\,\mu_h \tag{2.13}$$

Where n and p refer to electrons and holes concentration, respectively, e is the electric charge, μ_e and μ_h are electrons and holes mobility, respectively. From the relation it can be figured that electrical conductivity could be increased as much as carrier concentration increased. Doping is an effective way for increasing the concentration of charge carriers. However, it cannot be done above a certain limit because this will affect Seebeck coefficient and results in reduction of its value. Seebeck coefficient is related inversely to carrier concentration by the following relation[12], [19].

$$S = \frac{8\pi^2\,K^2}{3\,e\,h^2}\,m^*\,T\,\left(\frac{\pi}{3n}\right)^{2/3} \tag{2.14}$$

Here n is the carrier concentration, m* is the effective mass of the carrier, K and h are Boltzman and plank's constants, respectively. Thus, carrier concentration should be optimized to a certain value to balance S with σ [28]. It is found that ZT could be optimized at a carrier concentration of 10^{19} to 10^{21} per cm^3. This value falls in the area of heavily doped semiconductors between metals and semiconductors as it is clearly

appeared in Figure 2.3. For this reason heavily doped semiconductors are the best for thermoelectric purposes [1], [4], [28], [29]. Other factor is the effective mass (m^*) which refers to the density of state. From relation (2.14), it appears that m^* is directly proportional to S. Increasing m^* helps increasing Seebeck coefficient. However, this is also limited by a decrease in electrical conductivity. Heavy carriers will move with low mobility resulting in low electrical conductivity. Effective thermoelectric materials should be in a range where a balance between high effective mass and high mobility could be achieved. Therefore, optimizing the value of power factor requires a certain balance between Seebeck coefficient and electrical conductivity [28]. Thus optimizing the values of properties is one way to enhance figure of merit.
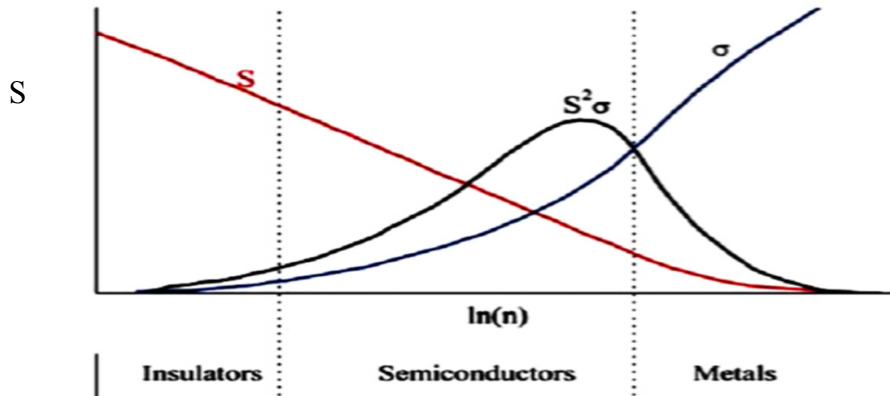
Figure 2.3: Variation of the Seebeck coefficient (S), electrical conductivity (σ), power factor ($S^2\sigma$), electronic thermal conductivity (k_e), and lattice (k_L) thermal conductivity on the charge carrier concentration n, for a bulk material [4]

Reducing thermal conductivity is another way of increasing ZT. ZT can reach infinity if thermal conductivity reaches zero. However, the reduction is limited to the lattice part of thermal conductivity as reducing the electronic part of thermal conductivity results in reduction of the electric conductivity. Wiedemann- Frenz law shows that electrical part of thermal conductivity (K_e) is related by directly to the electrical conductivity (σ) [1].

$$K_e = \sigma\, L\, T \tag{2.15}$$

Where L is Lorentz factor $2.4 \cdot 10^{-8}$ for free electrons and vary with carrier concentration [1].

According to all these complications and interrelation between thermoelectric properties, the best way to get good thermoelectric materials is by designing a material in a way that

help in decoupling the interrelation between their properties.

Most of the efforts done are focusing on reducing the lattice part of thermal conductivity by increasing the scattering of phonons at several scattering centers.

To achieve that, one of the following approaches could be followed:

1- Alloying: where some lattices sites of matrix material is substituted with different atoms. These guest atoms help in scattering the phonons which leads to reduction in lattice thermal conductivity. This method is an effective way specially when the ratio of the guest atom to the matrix atom is large [30].

2- Phonon rattling: where the guest atom can rattle and scatter the phonons by oscillating in an opened cage material structure. Unlike the case of alloying where the guest atom is totally bonded to the crystal, the guest atom that rattles the phonon is weakly bonded to the cage structure. This way could be achieved in materials with (phonon – glass electron – crystal). These materials behave like glass with low lattice thermal conductivity and like crystals with high electrical conductivity. Skutterudite and Caltherates are examples of these materials [1], [2], [12], [30].

3- Nano-structuring: where high densities of interfaces and grain boundaries are produced resulting in much phonon scattering and hence reduction of lattice thermal conductivity [30]. This will be discussed in details later.

2.3 Nano-structuring

Nano-structuring is an effective way that help in enhancing figure of merit [5]. The first use of the concept of low dimensional materials inorder to enhance figure of merit was in 1990 [31], [32]. Nano-structuring can be achieved by one of two ways: 1) reducing the scale of the material to the nano-range. 2) introducing nano-inclusions in the matrix material. As it is difficult to decouple the properties in bulk materials, Nanostructuring shows an excellent way to enhance figure of merit by several aspects [19].

1- Quantum confinement effect, where the electronic structure is changed. The number of energy states is reduced and band gab is increased. This is theoretically suggested that will result in sharp peaks and enhance Seebeck coefficient [33], [34] therefore increases thermopower [35].

2- Nano-structuring leads to increase the density of interfaces and boundaries that help mainly in reducing the lattice part of thermal conductivity. These interfaces coming from the presence of nanoinclusions or from grain boundaries that play an important role in increasing the scattering of phonons as illustrated in Figure 2.4. Phonons with mean free path longer in one or more dimensions than the nanostructure will be scattered effectively [36]. This will not affect the carrier mobility as the mean free path of carriers is few nanometers while for phonons it is from several nanometers to hundreds [4], [37].
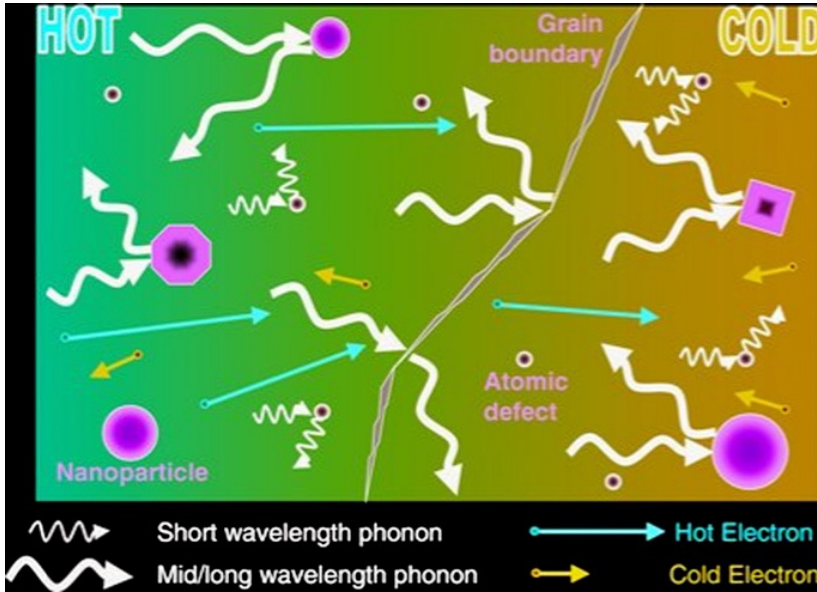
Figure 2.4: Schematic diagram illustrating the scattering of phonons and the transport of hot and cold electrons inside a thermoelectric material[22]

It is obvious from equation (12) that decreasing l will result in decreasing the lattice part of thermal conductivity. Generally, the transfer of heat through the lattice is affected strongly by the crystal structure. Any lattice disorder and all length- scale structures like vacancies, defects or grain boundaries result in phonon scattering [4], [38]. It is much more difficult for heat to move in low dimensional materials than electrons [39]. Grain boundaries and interfaces also can act as traps to filter the carriers that have low energy. This helps in enhancement of Seebeck coefficient by decreasing the average heat transported per carrier [40] as it appeared in Figure 2.5 [5], [28], [36]. All these effects will result in enhancement of ZT.
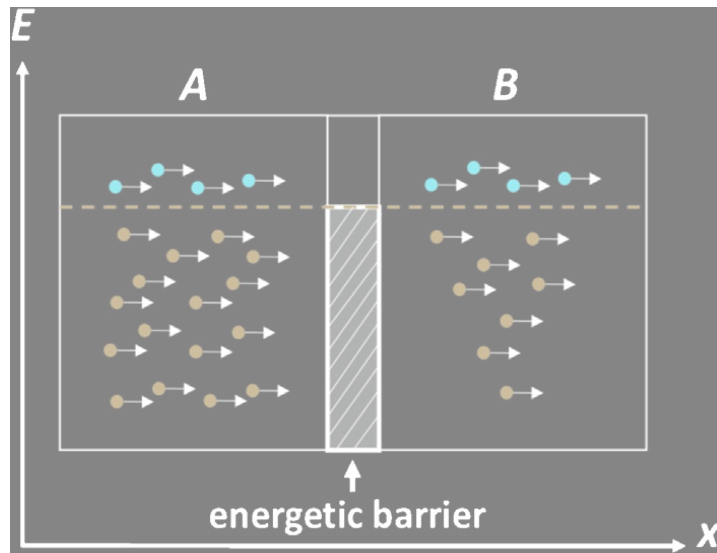
Figure 2.5: Electron energy filtering mechanism. Low charge carriers are filtered by the boundaries of the grains [117]

2.4. Thermoelectric module: device

Thermoelectric module which is the building block of thermoelectric system [41] consists of multiple of thermocouples. Each thermocouple consists of two legs of thermoelectric material. One is n- type with free electrons as main carriers and the other is p-type with holes as the main carriers. These thermocouples are connected electrically in series through metallic electrodes called bands while they are sandwiched between two ceramic plates with high thermal conductivity to allow them be thermally in parallel and low electrical conductivity. Thermoelectric module is represented in Figure 2.6 [28], [42].
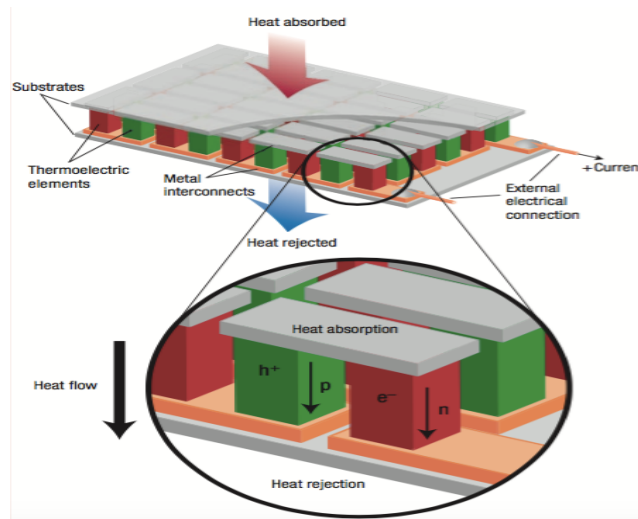
Figure 2.6: : Thermoelectric module [28]

Such an arrangement has an advantage of increasing the operating voltage and reduces current losses from electrical resistance of wires and interconnects [43]. While these parts form the basic array of the module, they are not the only parts that should be considered when discussing the device efficiency. Other components like the heat sink and cooling systems are also contributing to the efficiency. The power produced by these modules could range from 1-125 W for single one to 5 KW for several connected modules [12], [44]. The working principle of these modules based on what we have discussed previously, Seebeck effect. When heat is applied on the top side of the module, charge carrier will diffuse to the bottom side. So heat will transfer in one direction. However, this is not the case for the electric current. Current will be generated on the top side of n-type while in p- type it will be generated on the bottom side, as it is illustrated in Figure 2.7 [28], [45]. This module could act as a thermoelectric generator and in this case it is

connected to an external load or device or as a cooler if it is connected to power source [42].
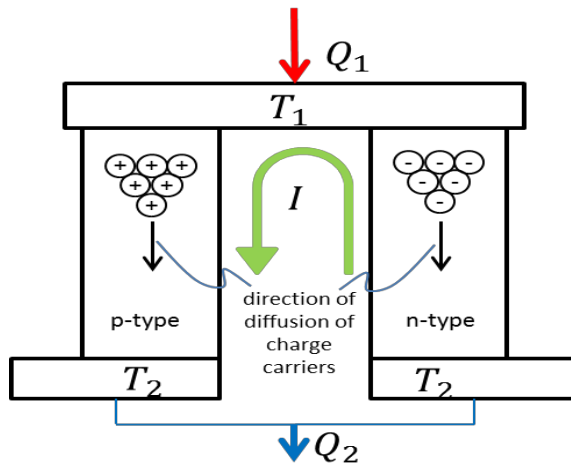
Figure 2.7: Direction of charge carriers diffusion and direction of current in thermocouple [42]

2.5 Thermoelectric efficiency

Thermoelectric module could be considered as a heat engine which its efficiency η can be determined by the ratio of useful output (W) to the input (Q_H) in terms of energy.

$$\eta = \frac{W}{Q_H} \tag{2.16}$$

Carnot engine is an ideal engine which gives maximum conversion efficiency. The

efficiency of thermoelectric device is related directly to Carnot efficiency, $\frac{T_h - T_c}{T_h}$ and to

figure of merit ZT_{av} of the material by the following relation:

$$\eta = \frac{T_h - T_c}{T_h} \left(\frac{\sqrt{1 + ZT_{av}} - 1}{\sqrt{1 + ZT_{av}} + \frac{T_c}{T_h}} \right)$$ (2.17)

Where T_h and T_c are the temperature of hot and cold ends, respectively. As ZT_{av}

increases, efficiency increases and tend to reach Carnot efficiency if ZT_{av} approach

infinity. Both ZT_{av} and temperature difference determine the final value of efficiency.

Figure 2.8 shows clearly the dependency of efficiency on ZT_{av} and ΔT [2], [18], [36],

[46].
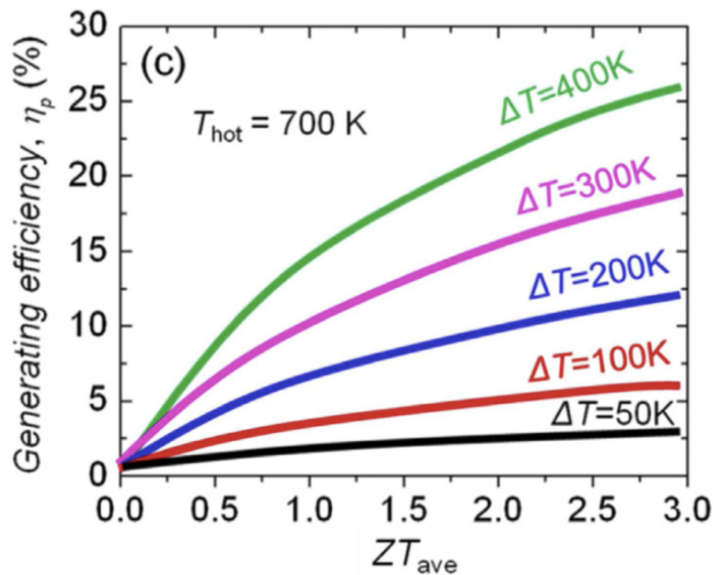
Figure 2.8: : Thermoelectric efficiency as a function of ZT [2]

38

2.6 Thermoelectric materials

2.6.1 History and development of thermoelectric materials

Since the discovery of Seebeck, Peltier and Thomson effects, thermoelectric materials are known. However, because of their low efficiency, no reported development was mentioned at that time [47]. In 1950's, the scientific basis of thermoelectrics were established and it was found that replacing metals with semiconductors will enhance the properties of thermocouple. A rapid development reported in the field where a first group of thermoelectric materials were developed. Bi_2Te_3, Pb-Te and SiGe bulk thermoelectric materials, were used in applications at low, intermediate and high temperature, respectively [4]. In the same period, there were some thinking that mechanical power generators and refrigerators could be replaced by thermoelectric materials but the results revealed that the efficiency remains less than the conventional machines [48]. A drop of progress in the field of thermoelectrics occurs in the period of 1960's and 1990's where thermoelectrics have little attention and the best materials were the $(Bi1_xSb_x)_2(Se_{1-y}Te_y)_3$ alloy family [29]. ZT of about 1 was reported at room temperature for those alloys and this value did not enhanced and makes a barrier for further development for a long time [49]. Later on, by 1990's, a committee of thermoelectrics were encouraged to improve the performance of thermoelectric materials and a break in the ZT barrier was achieved. Most of the efforts was done in order to reduce the lattice part of thermal conductivity by increasing the scattering of phonons. This could be achieved through nano-structuring or by looking for complex structure materials [47]. So historically, thermoelectric materials

started from simple metals to conventional bulk semiconductors reaching the complex

bulk structure material ending with low dimensional materials [50]. According to the

enhancement in ZT with time, thermoelectric materials could be divided to three groups

as in the Figure 2.9. The first group where ZT reached 1 in the period from 1960 to

1990's. The second group is ended by approximately 2010 where the effect of nano-size

start to enhance thermoelectric properties results in a ZT value reach 1.7. The last period

is under development for bulk thermoelectric materials and new technologies pushes ZT

to higher than 1.8. The goal for scientists in the field of development is to find a trend

where both low cost and high performance thermoelectric materials could be produced

[2].
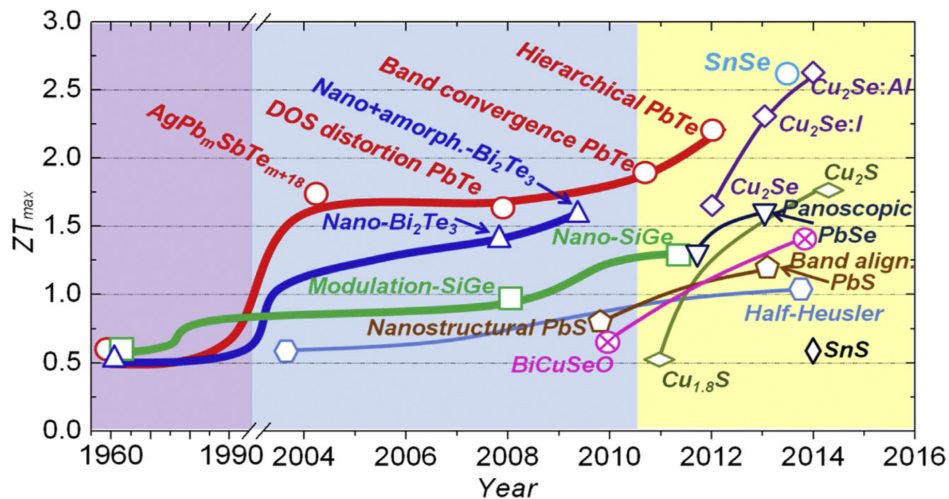
Figure 2.9: ZT of thermoelectric materials as a function of year [2]

2.6.2 Effective thermoelectric materials

Discussing in terms of material type, metals and insulators are excluded from thermoelectric materials as the first have low Seebeck coefficient and the second have poor electrical conductivity [51]. Heavily doped semiconductors are the most suitable ones as mentioned before [29]. Effective thermoelectric materials imply high figure of merit. This cannot be achieved unless high power factor or low thermal conductivity is satisfied in the interested material. Many approaches are followed to enhance Seebeck coefficient including: energy filtering, quantum confinement, and modifying the band structure. Low thermal conductivity could be found intrinsically in some materials that have complex crystal structure, large molecular weight or weak chemical bonding [21] or could be achieved in bulk alloyed materials. Another way to reduce lattice thermal conductivity is nano-structuring [2]. Nano-structuring could enhance ZT by either taking the material itself to nanoscale or embedding nanoscale constituents in the bulk matrix like nanocomposites [49]. According to the grain size, thermoelectric materials can be divided in three main classes, either nanoscale material, bulk nanostructured material or conventional thermoelectric materials and they will be discussed in more details in the following sections [4]. It is worth mentioning that combination of two of these groups could give a new group that has enhanced thermoelectric properties. However, thermoelectric materials is a large family and can be divided under different categories. Some of these categories are summarized in Figure 2.10.
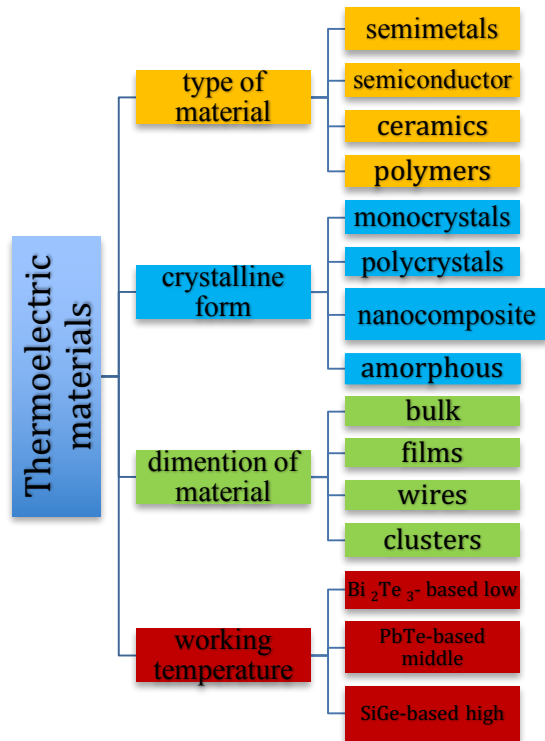
Figure 2.10: Diagram representing several thermoelectric classifications

2.6.3 Conventional thermoelectric materials

Low lattice thermal conductivity has a significant effect on the effectiveness of certain material as a thermoelectric one. Away from the resort to nanotechnology, low lattice thermal conductivity could be achieved, as previously mentioned, in alloys where the mass difference could help in scattering phonons [43]. SiGe alloys were considered as an affective thermoelectric materials for space applications since 1970s because of their low lattice thermal conductivity [52]. Bismuth Telluride and lead telluride conventional alloys

are also used as bulk materials for thermoelectric applications with ZT values reported between 0.8 and 1. An enhancement in thermal conductivity is also achieved in materials with complex crystal structure that follows Slack's concept of phonon-glass electron-crystal (PGEC) materials. These materials like Skutterudites, Clathrates and complex Zintal compounds could separate the electron crystal where it has high mobility from the phonon glass with low thermal conductivity [21], [29]. Skutterudites and Clathrates have a cage- like structure with voids that can be filled with guest atoms like rare- earths, alkaline earths, or alkali metals. These atoms are bonded weakly to the rest structure so they can rattle inside the crystal causing phonon scattering and limiting thermal conductivity [29], [53]. Filled Skutterudites materials exhibit good thermoelectric performances, for example $Yb_{0.19}Co_4Sb_{12}$ has ZT = 1.14 at 640 K, $Ca_{0.18}Co_{3.97}Ni_{0.03}Sb_{12.4}$ shows ZT of 0.99 at 800 K, $Ba_{0.24}Co_4Sb_{12}$ with ZT of 1.1 at 850 K and ZT of 1.4 was achieved in $CeFeCoSb_3$ at around 1000 K. Clathrates show high ZT values in some compounds, ZT = 1.35 at 900 K was reported for $Ba_8Ga_{16}Ge_{30}$ and 0.72 in the case of n-type $Sr_8Ga_{15.5}In_{0.5}Ge_{30}$ at 800 K. Complex Zintal compounds contain a combination of ionic and covalent bonds leads to complexity in the structure and hence to reduction in thermal conductivity. One example is $Yb_{14}MnSb_{11}$ shows ZT of 1.1 at 1275 K [51] which is almost twice that of p-type SiGe. This make it an interesting material for spacecraft uses at NASA program [28]. For both alloys and complex structure materials, further enhancement could be achieved by nano-structuring, whether by nano-inclusion embedding or producing the materials in the nanoscale [48]. One of the best methods for

achieving an effective thermoelectric material is to combine the complexity of the structure with nano-structuring [28].

2.6.4 Nanoscale thermoelectric materials

Low dimensional thermoelectric materials either with nano or even with micro scale were proved experimentally to exhibit enhancement in figure of merit [54]. It was difficult for a long period of time to increase figure of merit more than 1 for conventional thermoelectric materials [55]. This low dimensionality could be achieved in the material itself or could be embedded as inclusions within a bulk matrix to produce nanocomposite. This help mainly in reducing lattice thermal conductivity by increasing phonon scattering at the boundaries and enhancing Seebeck coefficient according to energy filtering effect of low energy carriers where grain boundaries act as energy barriers [46], [49], [56], [57]. Several forms of intrinsically nanomaterials could be produced like nanotubes, nanorods, nanowires, nanoparticles, thin films quantum wells and super-lattices [12]. Enhancement of ZT as a result of increasing boundaries was realized first for SiGe polycrystalline alloy where the grains have less than 5 μm size. Rowe et al. [52] reported significant reduction in lattice thermal conductivity and hence an enhancement in figure of merit was achieved [56]. Si is considered as a poor thermoelectric material with ZT of 0.1 at RT. However, it is reported that ZT up to 0.6 at RT and 1 at lower temperature could be achieved if the material is produced as nanowires [7], [17], [43]. Pb-Te quantum well also shows an enhancement in lattice thermal conductivity and exhibit ZT of 1.2 at RT [59]. Zhaou et al. [60] prepared $Bi_{0.485}Te_{0.515}$ nanowires and figured out that lattice thermal conductivity

is reduced by 28% to 57% compared to bulk one [60]. Ultra-thin nanowires n-type

$Bi_2Te_{2.7}Se_{0.3}$ were prepared by chemical method by Zhang et al. and ZT of 0.95 is

achieved which is 13 % higher than the conventional one [61]. The highest value of ZT

was predicted by Hicks and Dresselhaus to be in super-lattices thin films. It was verified

by Venkatasubramanian et al. [6] and high ZT of 2.4 and 1.2 were achieved for p-type

and n-type Bi_2Te_3/Sb_2Te_3 super-lattice structures, respectively, which is much higher than

any conventional material [46]. $PbTe/PbSe_xTe_{1-x}$ super-lattices also showed ZT

enhancement due to phonon scattering [62].

2.6.5 Nanostructured bulk thermoelectric materials

Although a significant success has been achieved in nanoscale thermoelectric materials,

the synthetic methods of producing these materials are difficult and of high cost. In

addition, the materials produced are difficult to be fabricated in a large scale and in large

quantities needed for commercial applications as all of thermoelectric devices used in

industry based in bulk materials [52], [58], [63], [64]. For these reasons, lots of work

done to develop high efficiency bulk nanostructured materials which could combine the

characteristic of nano-dimensional materials along with the production of bulk samples

by an easy and low cost techniques with sufficient amount for commercial uses[58][17].

These materials are either produced as powders with nanograins by several methods

including capor deposition, chemical reactions or through coarse raw materials'

processing methods like mechanical allouing / ball milling and melt spinning [39][17].

Enhancement in figure of merit for nanostructured bulk materials was achieved in several

materials. A peak of 1.3 ZT was reported for n-type SiGe nanostructure bulk alloy at 900

^{0}C [3]. Bathulal et al. [25] reported the highest ZT of 1.5 for the same alloy at the same

temperature while for p-type Si-Ge alloy, ZT of 0.95 was reported which is 50% higher

than the bulk [65]. Although these values were achieved in silicon nanowires as

mentioned in the previous section, the advantages of easily scaled up nanostructured

bulk materials make them much interested for industrial applications [65].

Nanocomposites, which take the advantages of lower dimensional structure, also

achieved high ZT compared to regular materials. Any type of nanostructure like

nanoparticles, nanowires, nanodots, etc can be embedded and disrupt the phonon path to

reduce lattice thermal conductivity [53]. P- type $Si_{80}Ge_{20}$ shows an enhancement in figure

of merit from 0.65 in bulk to 0.95 in nanocomposite [65] and from 0.9 in bulk n-type to

1.3 in nanocomposite [25], [66]. One of the highest ZT value was reported for PbTe -

$AgSbTe_2$ nanocomposites to reach 2.1 near 800 K [52]. Pb-Te nanocomposite showed

enhancement in thermal conductivity compared to regular one when embedded with

nanoinclusions . Nanoinclusion of lead and antimony in Pb-Te result in doubling ZT to

reach 1.5 at 700K while the presence of 2% of antimony in the matrix result in reduction

of lattice thermal conductivity by factor of 3. Nanostructuring shows also an

enhancement in figure of merit in complex structure thermoelectric materials due to

reduction in lattice thermal conductivity [63]. Hot pressed $CoSb_3$ powder containing nano

and micro-particles lead to 54% enhancement in figure of merit at 700 K [58] while

nanoinclusion-containing $CoSb_{2.70}Te_{0.25}Sn_{0.05}$ has a *ZT* of 1.1 at 550° [28]. Maximum

value of ZT of 0.7 was achieved in n-type $(Ni,Co)_4Sb_{12}$ nanocomposites and 1.2 in

$Yb_xCo_4Sb_{12}$ nanocomposites [66]. Bulk undoped nanostructure Bi_2Te_3 which is prepared by Saleemi et al. [67] shows ZT of 1.1 at 340 K according to the enhancement of power factor compared to state of art material while a maximum ZT of 1.56 at 300 K was achieved for p-type $Bi_{0.52}Sb_{1.48}Te_3$ bulk material which is more than 50% improvement compared to the state of the art Bi_2Te_3 materials [7]. Zhao et al. [68] produce Bi_2Te_3 nanocomposite by embedding Bi_2Te_3 nanotubes into Bi_2Te_3 matrix, this compound shows an enhancement in figure of merit to reach 1.25 at 420 K while ZT of 1.4 was achieved in p-type bismuth telluride nanocomposite at 250 ^{0}C [3].

2.7 Synthesis techniques

Lot of methods are used for producing nanoscale thermoelectric materials. Hydrothermal methods to produce nanoparticles and nanotubes [69], electrochemical deposition for nanowires and superlattices nanowires [70]. Thin films and superlattices production technique like Molecular Beam Epitaxy (MBE) and Chemical Vapor Deposition (CVD) are two techniques used for production of thin-films. The produced thin- films materials are with high performance thermoelectric materials. Although these methods could produce materials with good thermoelectric properties, it is not enough to consider them as effective methods as they may suffer from several disadvantages like complexity, high cost or may not able to produce materials in bulk forms that are suitable for commercial applications [7], [71]. The highest ZT was reported for Bi_2Te_3/Sb_2Te_3 super-lattice [6] but with high cost. It requires a precise controlled to achieve high ZT, and also to achieve the desire composition. This process structures limits the thickness of the deposited films to

few micrometers which allow high heat transfer compared with traditional large scale devices [72], [73]. Several solution chemical synthesis are used to produce nano materials including several thermoelectric compounds like Bi_2Te_3 and its alloys, Bi_2S_3, PbTe, PbSe and BiSb [74]–[76]. Although some of these methods are effective for producing nano thermoelectric materials and some of them could produce large quantities with low cost [56], [74], [75], [77], [78] but at the same time they have several disadvantages. Some of chemical synthesized materials reported are produced with too large nanostructure size (up to hundreds nanometers), others suffer from difficulty of assembling them into pure materials which lead to bad thermoelectric properties [79]. In addition, chemical processes need careful designing the reaction agents and controlling the synthesis parameters [74] and they affect the environment as they based on chemicals for production process. Among different synthetic processes, two methods are used to produce Bi-Te in the bulk forms, ball milling with subsequent sintering to produce bulk nano-powder and melt spinning to create nanostructure ribbons [80] .Tang et al. [68] used the melt spinning to produce Bi_2Te_3 bulk materials with layered nanostructure and ZT of 1.35 at 300 K was obtained while ZT reaches a maximum value of 1.56 at the same temperature for the p-type $Bi_{0.52}Sb_{1.48}Te_3$ bulk material produced by the same method. However, it produces a material with unique microstructure with nano-crystalline domains in the amorphous matrix. Zone melting ingots were used as starting materials for melt spinning where this step can be avoided in the mechanical milling technique by using elemental powder as starting materials [81].

2.7.1 Mechanical alloying/ball milling

Mechanical alloying started as an industrial necessity in 1966 for aerospace industry. Mechanical alloying with high energy ball milling is a powerful top down dry powder processing method for semiconducting solid solution and alloys formation [17], [82], [83]. It has the ability to produce large quantities of nano-powders with size as small as several nanometers [58], [66]. These nanostructure materials are generated by severe plastic deformation on the coarse grained material by repeated mechanical impacts during milling [82], [84]. The combination of low cost [8], simple equipment with method works at room temperature and the production of nanostructure materials in a short time with oxygen and impurity free are all advantages of mechanical alloying [46], [84]. Shaker mills such as SPEX mills are the most used for laboratory and for research uses and can mill about 10 to 20 g of powder at a time. They have one vial that contains the sample and the balls and shakes thousands time per minute [83] as illustrated in Figure 2.11.
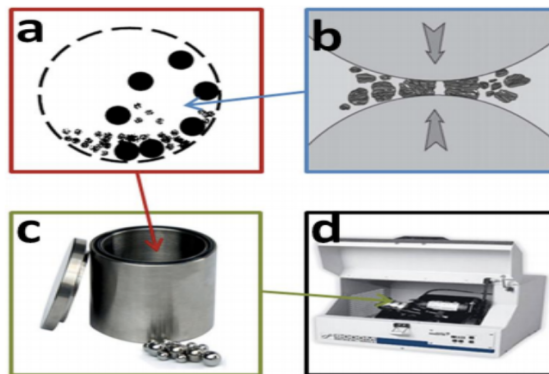
Figure 2.11: Schematic view of mechanical alloying. (a) ball-powder movement during milling, (b) ball-to-powder interaction, (c) milling media, balls and vial, (d) SPEX 8000 mill

The produced materials are homogeneous, strong and exhibit low thermal conductivity while keeping the electron transport properties. They show even an enhancement in power factor, which in result show significant enhancement in figure of merit comparable to conventional bulk ones. Nanostructured SiGe alloy that produced by ball milling exhibit high figure of merit [25], [65] while Pb-Te alloy prepared by ball milling shows enhancement in thermopower comparable to $PbTe/PbSe_xTe_{1-x}$ quantum dot super-lattices [58]. Maximum ZT value of 1.3 was achieved by producing nanostructured p-type bismuth telluride material from elemental chunks using ball milling [73] while a peak of 1.4 was achieved when using ingot of the alloyed crystal as starting material [85]. This is the best value was reported for bulk nanostructured Bismuth Telluride materials. It is also higher than ZT value reported for Bismuth telluride thin films and nanowire produced by potentiostatically electrodeposition technique where the maximum ZT value achieved was 0.9 at 350 K [70]. Although mechanical milling is simple but it is effective for synthesis of complex composition materials. Polycrystalline $Ag_{0.8}Pb_{18+x}SbTe_{20}$ bulk material was produced by Wang et al. [86] with ZT= 1.37 at 673 K. Nice comparison between different preparing methods of bulk bismuth telluride is shown in Figure 2.12. It is obvious that bismuth telluride material produced by ball milling shows the highest figure of merit compared to other techniques.
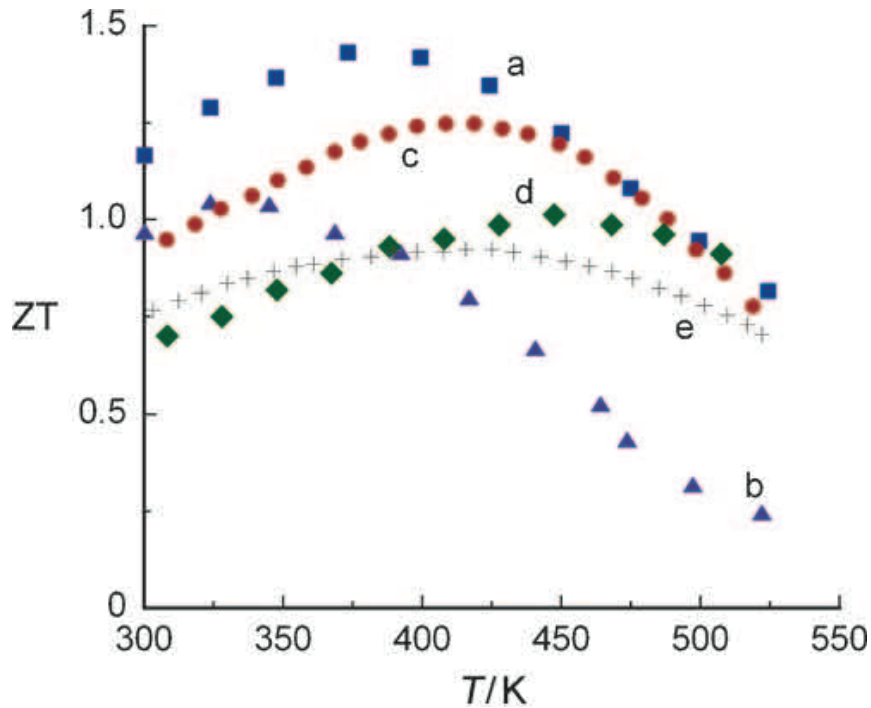
Figure 2.12: : Figure of merit (ZT) as a function of temperature for bulk Bi$_2$Te$_3$ materials prepared by a) ball milling with hot pressing, b) zone melting, c) melt spinning with SPS, and d) hydrothermal synthesis, and e) the state-of-the-art Bi$_2$Te$_3$ prepared by zone melting (for comparison) [63]

2.7.2 Hot pressing

Hot pressing is a compaction method used to produce full dense compacted powder material with controlling its fine structure. The working principle of this method depends on application of uniaxial pressure in one or two opposite directions as in Figure 2.13 while the sample is heated at the same time under vacuum or inert condition to prevent oxidation. This process will help in reducing the processing time as well as the temperature compared to traditional sintering.
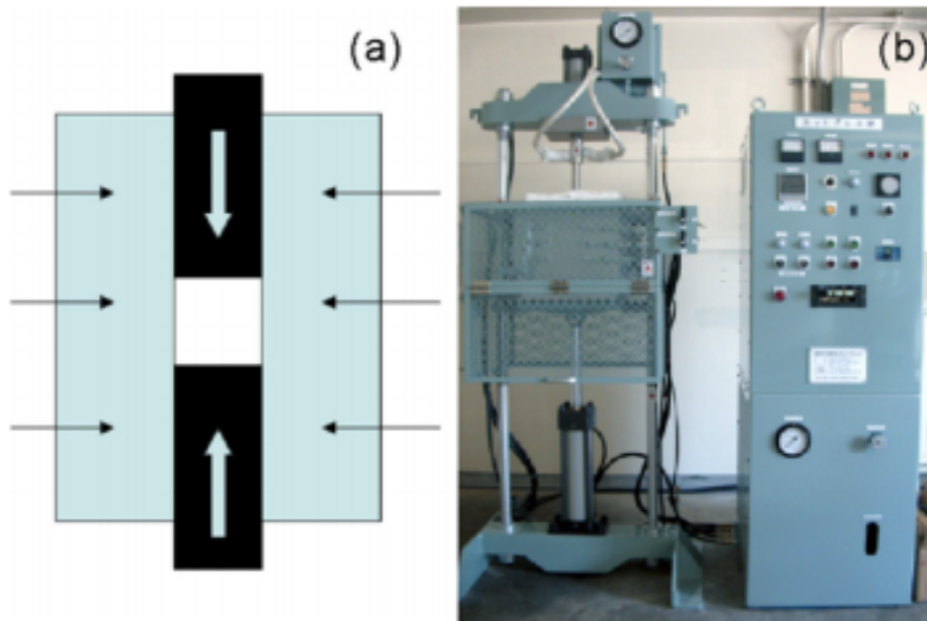
Figure 2.13: (a)Schematic of hot-pressing setup and (b)hot-pressing equipment with temperature and pressure controller [9]

Hot pressing machine can work with high temperature and uniaxial load up to 25 tonn, which is able to densify different types of materials. Hot pressing suffers from the problem of grain coarsing. However, suitable combination of pressure and temperature conditions helps effectively in maintaining nanostructuring [9].

2.8 Bismuth telluride based materials

Among all effective thermoelectric materials that have been discussed previously, Bi-Te based materials are the best and most commercial materials used for cooling refrigerator and power generator that have highest figure of merit at low temperature (200 – 400 K)

and their devices can support up to 500 K [10]. Bi-Te was discovered by H.J Coldsmid and coworkers in UK and reported as an effective thermoelectric material since 1954 [59]. Bismuth telluride is a narrow band gap semiconductor. Its crystal structure belongs to rhombohedral with space group R3m. The crystal unit cell consists of five atomic layers with continually repeated (Te_1-Bi-Te_2-Bi-Te_1) consequence, connected weakly by van der Waals interaction along C- axis as shown in Figure 2.14 while the interlayer interaction between Bi and Te is much stronger as they bond to each other by covalent and ionic bonds. This crystal structure results in anisotropy where mechanical properties, thermal and electrical conductivity are different within different directions in the unit cell. The crystal is easily cleaved along the direction perpendicular to C axis and thermal and electrical conductivity are two and four times higher in the same direction [63], [68], [73], [87].
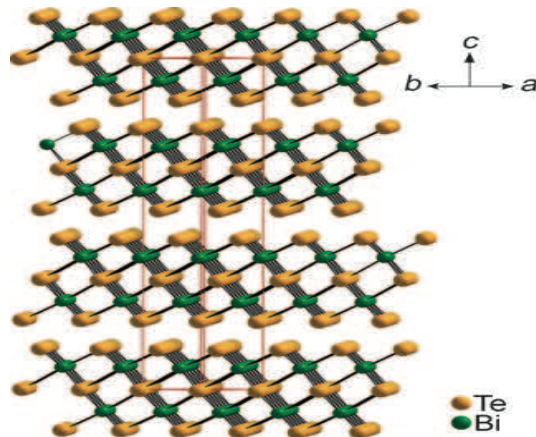
Figure 2.14: Bismuth telluride crystal structure [63]

Bi-Te alloys are prepared by traditional zone melting method and got ZT close to 0.8 [88] but it is found that when it is alloyed with other materials to get p- or n-type, ZT shows significant enhancement as charge carriers increases. Generally, heavily doping several donor or acceptor atoms is a common way used to enhance the electrical properties [89] and hence enhancing figure of merit [90]. For instance, Cs Bi_4Te_6 shows an enhancement in thermoelectric properties at low temperature compared with Bi_2Te_3 [91] but to make strong p-type, Bi is replaced by Sb while for strong n-type, Te is replaced by Se. These two elements were found to be an appropriate choice for carrier concentration adjustment. The highest ZT value obtained for p and n, $Bi_{0.4}Sb_{1.6}Te_3$ and $Bi_2Te_{2.7}Se_{0.3}$ alloys [46]. ZT of 1 limits Bismuth Telluride applications for a long time till recent studies show that nano-structuring could enhance its thermoelectric properties [67]. From literature, the highest ZT for bismuth telluride based materials produced by several methods are achieved around room temperature [78], [90], [92], [93] while for med temperature range (600-800 K) Pb-Te shows the highest ZT [94], [95] and Si- Ge operates effectively at high temperature [25], [65], [72], [96], [97]. Other materials with complex structure [98], filled Skutterides, Calthrates and metal oxides are effective thermoelectric materials but at temperatures higher than room temperatures [40]. Figure 2.15 shows the graph of ZT for different thermoelectric materials at different temperature ranges. It is obvious that nanostructure Bismuth telluride material shows the highest ZT at low temperature [63].
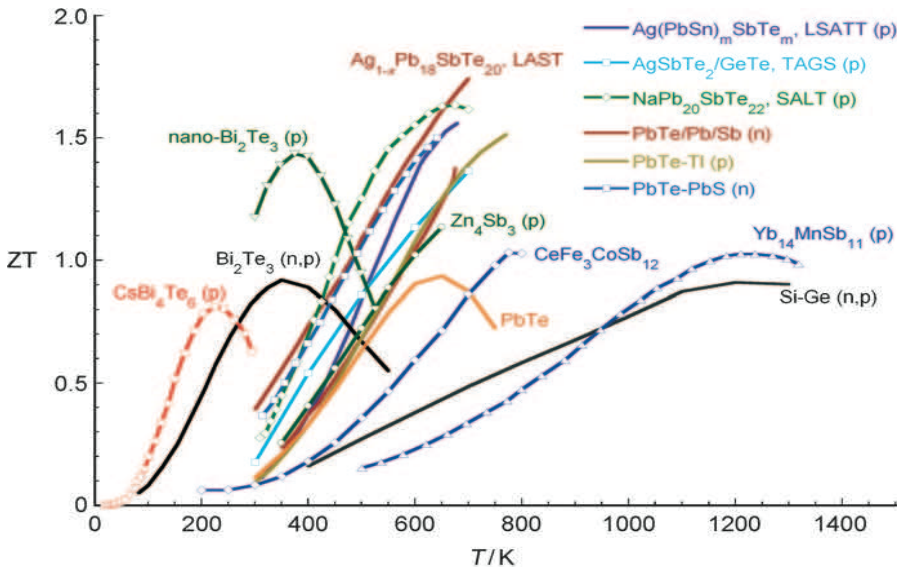
Figure 2.15: : Plot of different thermoelectric materials with ZT values at different temperatures [63]

CHAPTER 3

Experimental work

3.1 Materials

- High purity Bismuth powder (99.99%).

- High purity Tellurium powder (99.99%).

- High purity Selenium powder (99.8%).

- High purity Antimony powder (99.999%).

All materials from Alfa Aesar Company.

3.2 Preparation method

Bulk nanostructured p-type ($Bi_{0.4}Sb_{1.6}Te_3$) and n-type ($Bi_2Te_{2.7}Se_{0.3}$) Bismuth Telluride material were fabricated by hot pressing of powder produced by mechanical alloying / ball milling of elemental powders.

3.2.1 Mechanical alloying/ ball milling

High purity commercial powder of Bi (99.99%), Te (99.99%) and Sb (99.999%) for p-type sample and Bi, Te and Se (99.8%) for n-type sample are used as raw materials. Appropriate quantities of elements were weighed in Argon filled glove box according to their composition ratio. The calculated weights for p-type ($Bi_{0.4}Sb_{1.6}Te_3$) are 0.6321g,

2.8948g and 1.473g for Bi, Te and Sb, respectively, while for n-type ($Bi_2Te_{2.7}Se_{0.3}$) are

2.6585g, 2.191g and 0.1507g for Bi, Te and Se, respectively with total of 5 g for each.

The powders are loaded in to stainless steel ball mill jar in High energy SPEX MILL-

8000 Mmachine which appears in Figure 3.1 with two different size balls have a total

weight of 50 grams. Balls to powder weight ratio was kept 10:1 during milling. The

powders subjected to mechanical alloying for 20 hours at room temperature under ultra-

high pure argon atmosphere to prevent oxidation. To study the milling evolution process,

three more samples of n-type material were weighed and milled for milling time of 1, 4

and 8 hours.
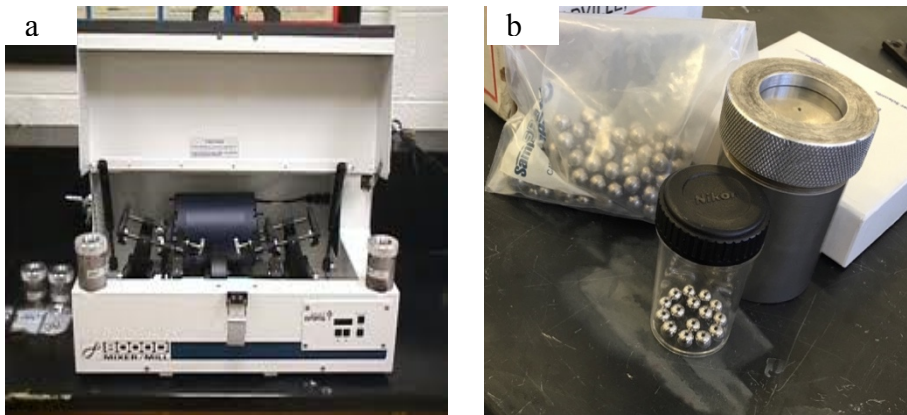
Figure 3.1: a) SPEX milling machine b) balls with steel vial

3.2.2 Hot uniaxial pressing

N- and p-type milled powders were pressed into bulk samples using hot pressing machine. Disk shaped specimen were produced by uniaxial hot pressing of the powder samples. Pressing done under Argon atmosphere and powder loaded into a tungsten carbide (WC) die as seen in Figure 3.2.
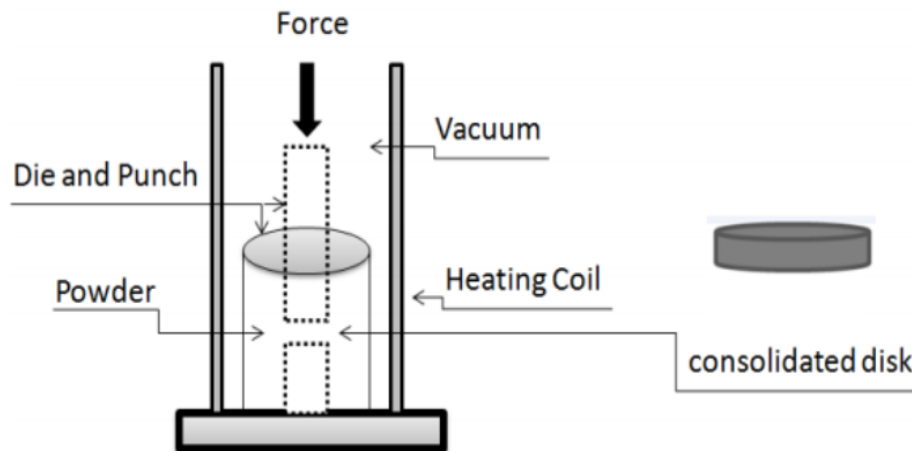
Figure 3.2: Hot pressed disk by uniaxial hot pressing

3.4 Characterization
3.4.1 Structural characterization

3.4.1.1 X-ray diffractometer

X-Ray diffraction is the most common technique for materials structural

characterization. It is very useful as materials properties are highly dependent on their

structure. The working principle depends on exposing the sample to focused X-ray beam

that is generated in a sealed tube. The crystalline structure of the sample is defined by

repeated planes of atoms which form the crystalline lattice. When the beam interacts with

the sample, part of it will be absorbed, part will be transmitted, part will be refracted and

part will be diffracted. The diffracted beam depends on the arrangement of the atoms in

different planes and the obtained diffraction pattern gives a good identification for the

crystal structure of the material. The position and intensity of each peak refers to a certain

phase of the material which is different from one material structure to another even if it is

made from the same atoms. The distance between the planes that formed the crystal

lattice can be measured using Bragg's law

$$n \lambda = 2d \sin \theta \hspace{4cm} (3.1)$$

where n is an integer representing the order of the diffracted beam, λ is the wavelength of

X-ray beam, d is the distance between adjacent planes of atoms (the d-spacing), and θ is

the angle of incidence of the X-ray beam. Set of d values provide a fingerprint of the

materials in the sample [99]. In our experiment, the crystallinity, phase structure of the

mechanical alloyed and annealed samples were analyzed by X-Ray diffraction (XRD)

investigation with Cu-Kα radiation. The sample was carried out using Rigaku Ultima IV Multi- Purpose X- ray Diffractometer which is illustrated in Figure 3.3. Parameters used were as follows: source current 20 mA, voltage 40 kV, wavelength is 1.5404 Å, continuous scan with scan rate of 0.5^0/ min and 2θ range from 10^0 to 100^0.

Figure 3.3: Rigaku Ultima IV Multi-purpose X-ray diffractometer

The average grain size and lattice strain were calculated using Averbach method. The grain size and lattice strain are calculated using the following equation

$$\frac{(\beta 2\theta)^2}{tan^2\theta} = \frac{\lambda}{D}\left(\frac{\beta 2\theta}{tan\theta \, sin\theta}\right) + 25 \, e^2 \tag{3.2}$$

where D is the grain size, θ is Bragg's angle (in radian), $\lambda = 1.54^0$, β is full width half maximum (in radian) and e is the strain.

3.4.1.2 Scanning electron microscopy

SEM is a powerful instrument used for microstructural surface analysis of solid objects. It is a high-resolution technique that could give large depth of field for and a 3-D appearance image. It can examine the specimen with high as well as very low magnification. SEM machine consists of several components: lens system, electron gun, electron collector, visual and recording cathode ray tubes and other electronics associated with them. The working principle of this technique depends on exhibiting the specimen to focus electron beam, which as result lead to several scattered signals from different thickness of the sample surface. Backscattered and secondary electrons are the main signals for SEM purposes as they varied according to surface topography [100]. In our investigation, the morphology and texture of the as milled p- and n-type samples at different milling time were observed using FEI Quanta 200 scanning electron microscopy (SEM) shown in Figure 3.4 via. Small amount of the powder from each sample were loaded on 5.7 mm diameter pan under 5 KV source voltage.

Figure 3.4: Quanta 200 scanning electron microscopy (SEM)

3.4.1.3 Transmission electron microscope

TEM is a characterization tool used to obtain information about the grains' structure, grain size and size distribution. The working principle of this technique depends on the transmission of focused beam of electrons through a sample. The use of electron beam helps in giving high resolution image. Dark and bright field images could be obtained and the contrast in the image depends on the amplitude and phase variation of the beam. The contrast is determined by the amount of the electron beam that can pass through a sample which is a function of thickness of the material and its type. More electrons are scattered if the atoms are heavy atoms [101]. In our experiment, the fine nanostructure of the samples was observed using TEM image and the grain sizes were measured. Bright and

dark field images were obtained using FEI TECNAI GF S-TWIN transmission electron

microscope shown in Figure 3.5. Samples were prepared using focused ion beam (FIB)

sample thinning.

Figure 3.5: Tecnai transmission electron microscope (FEI)

3.4.2 Thermal characterization

3.4.2.1 DSC analysis

Differential Scanning Calorimetry (DSC) is the most common technique to study the thermal behavior and the phase transition of the materials. The working principle of the machine depends on subjecting the sample to a controlled temperature program and measuring the heat flow rate either into or from the sample as a difference compared to a reference [102].
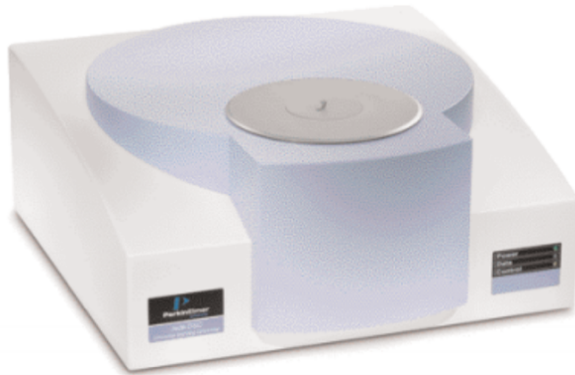
Figure 3.6: Perkin Elmer Jade DSC

In our experiment thermal behavior of As-milled n- and p-type samples was studied using Perkin- Elmer jade differential scanning calorimeter shown in Figure 3.6. Each sample has gone through a cycle of heating – cooling - heating at heating rate of 10 °C/min from RT to 430 °C.

3.4.2.2 Annealing

P- and n-type samples were annealed in split tube furnace. Annealing was done under Argon atmosphere to prevent oxidation. Small amount of the powder from both samples were loaded into ceramic boats and placed in the middle of the furnace tube. The samples have gone through heating from RT to 300℃ then cooled down. Annealing was done to study the effect of heat on the structure and the grain size of the material to determine the suitable pressing conditions.

Figure 3.7: Split tube furnace

3.4.3 Mechanical properties characterization

3.4.3.1 Vickers micro-hardness test

Hardness test is done to give good information about mechanical properties of the material. Vickers hardness test is an accurate method that is capable of testing hard as well as soft materials. It is also known as diamond pyramid hardness. The working principle depends on indenting the material with a pyramid diamond indenter which is subjected to a certain force on its squared base. The average of the diagonals of indentation left in the surface of the material after removing the load is calculated. The surface area of indentation is calculated and the hardness is calculated by dividing the load by surface area [103], [104].

In our investigation, n-and p-type as-milled and annealed materials were compacted into disks. Vickers micro-hardness test was measured by using micro-hardness tester FM-ARS9000 with a diamond pyramid indenter. A load of 0.245 N were used and five measurements at different locations on the samples surfaces were performed in order to determine an average hardness value. The measurements were done at RT.

The Vickers micro-hardness, Hv (in MPa) is evaluated using the following formula:

$$H_v = 1.854 * P/d^2 \tag{3.3}$$

Where P = Load applied during the test in SI units and $d = (d_1 + d_2)/2$ in SI units.

Figure 3.8: Vickers micro-hardness tester

3.5 Thermoelectric properties characterization

All electrical properties (Seebeck coefficient α, electrical conductivity σ, and thermal conductivity) for the n- and p-type thermoelectric materials were determined within a single measurement run at the analytical instrumentation facility at North Carolina State University. The system provides the ability to change the temperature on either side of the device that allows the same temperature differential to be attained at different operating temperatures. Peltier unit was designed to provide quick heating to the samples. This system design is based on the system proposed by Schwyer et al. [105]. Schematic diagram of thermoelectric properties measurements setup is illustrated in Figure 3.9. The average value of each property were calculated after doing the measurements for two samples from

both n-and p-type materials. Since we mainly consider the utilization of these thermoelectric materials within a relatively low range of temperature, the transport properties were measured at temperature range from 25 °C to 100°C. The samples used for transport properties measurements were the compacted discs after hot pressing. The diameter of the samples was 10 mm with a thickness of 4 mm. Four perpendicular cuts with a width of 1 mm were introduced into each sample in order to minimize error measurements, as shown in Figure 3.10. Four ohmic contacts were arranged with near mirror symmetry on the boundary of the sample surface using gold micro wires at points A, B, C, and D, as shown in Figure 3.10. The electrical resistivity (ρ) was measured as a function of temperature using the well-known van der Pauw method [106]. The electrical resistivity is given by:

$$\rho = \frac{\pi t}{ln2} R_{AB,CD} \tag{3.4}$$

Where t is the thickness of the sample and $R_{AB,\ CD}$ is defined by:

$$R_{AB,CD} = \frac{V_{CD}}{I_{AB}} \tag{3.5}$$

where, V_{CD} is the voltage drop between probes C and D when the electric current (I) is passed between probes A and B, see Figure 3.10. The same set up shown in Figure 3.9 was also used to measure the Seebeck coefficient of the n- and p-type samples within the same temperature range. Two copper blocks sandwiched the sample under ultra-high purity Argon atmosphere. A heating element rapidly increases the temperature of one copper block and a set of thermocouples were used to detect the temperature difference (ΔT) across

the sample. The corresponding voltage difference (ΔV) was measured simultaneously across the sample. Then the Seebeck coefficient was calculated according to equation,

$$S = \frac{\Delta V}{\Delta T}$$

Within the same temperature range, from 25 °C to 100 °C, the thermal conductivity of the n- and p-type samples were measured in the same orientation as the electrical resistivity and the Seebeck coefficient. As shown in Figure 3.11, heat flow was measured using calibrated Q-meter. If all the heat supplied to the source, Q, is conducted along the sample of uniform cross section, A, and distance, L, between temperature sensors, see Figure 3.11. The total thermal conductivity (K_{tot}) between points 1 (T_h) and 2 (T_c) separated by distance L is given by [107]:

$$K_{tot} = \frac{Q\,L}{\Delta T\,A} \tag{3.6}$$

Where $\Delta T = T_h - T_c$, this method is most widely used for measurements at low temperatures and it assumes that the temperature is uniform through the sample cross section.
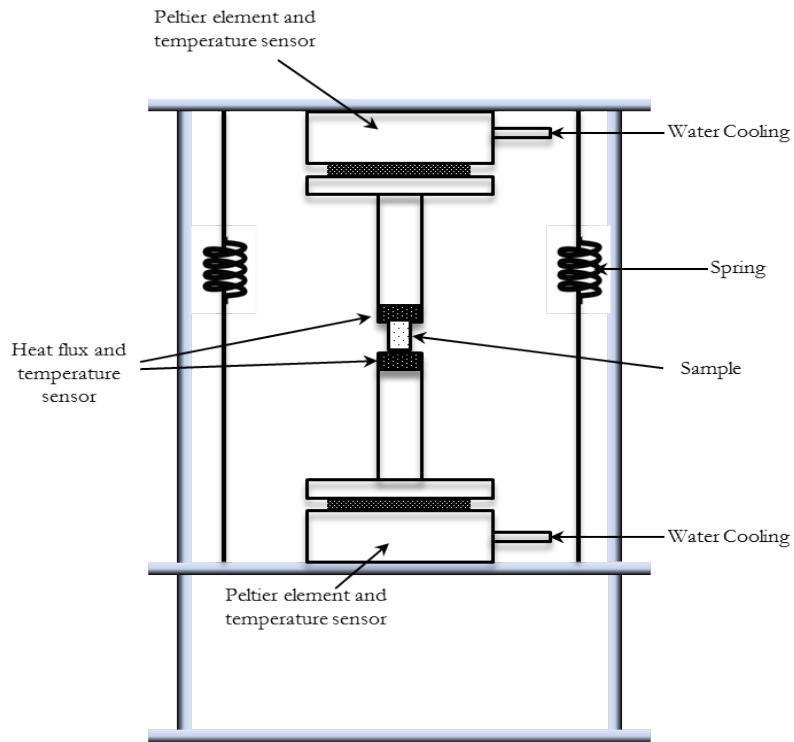
Figure 3.9 A Schematic diagram for the thermoelectric properties measurements setup
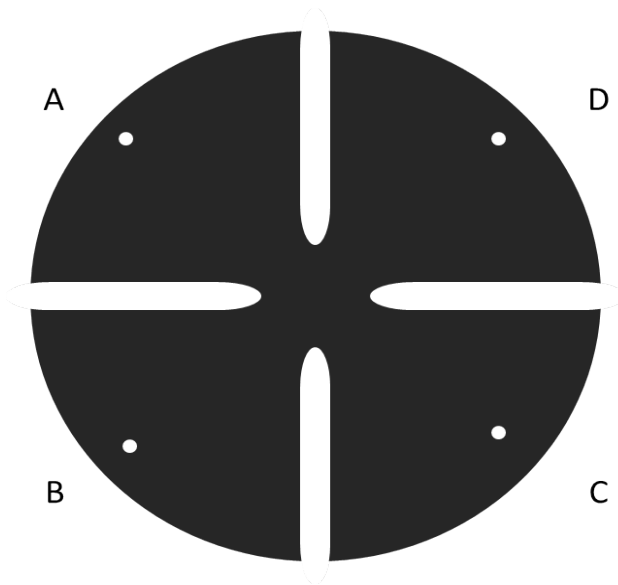
Figure 3. 10 : Disk sample with four perpendicular cuts with a width of 1 mm
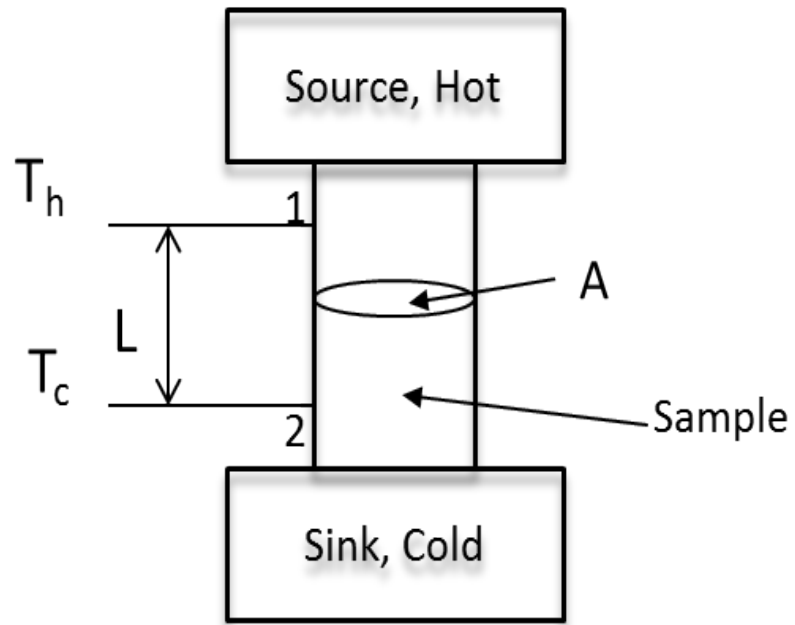
Figure 3. 11: Thermal conductivity measurement for a disk sample of A cross section area and length L

CHAPTER 4

Results and discussion for n-type Bi-Te material

4.1 Structural characterization of n-type Bi-Te material

4.1.1 X-Ray diffraction analysis of n-type Bi-Te material

XRD patterns for as-milled n-type samples at 1, 4, 8 and 20 hours of milling time are shown in Figure 4.1. The patterns show the evolution of alloying process. As can be seen, almost complete alloying of the elemental powders occurred as early as 1 h. Similar behavior of early alloying reported by S.A. Humphry-Baker and C.A. Schuh [108]. As illustrated in Figure 4.1, the patterns at 1, 4, 8 hours contain some small peaks that are not matched to single phase of ($Bi_2Te_{2.7}Se_{0.3}$), which indicate that the materials are not completely alloyed. However, after 20 hours of milling all the small extra peaks disappeared. The final XRD pattern is indexed to rhombohedral Bi_2Te_3 single phase. The progressive broadening of the peaks with milling time is clearly observed indicating the fine nano- size of the grain boundaries. The grain size and lattice strain were estimated using Averbach method. Figure 4.2 shows linear fit of $\frac{\beta2}{tan2\theta}$ against $\frac{\beta}{tan\theta sin\theta}$ for all measured peaks. The intercept and the slope of the linear fitting was used to calculate the grain size and the lattice strain, respectively. The calculated grain size was found to be 18 nm and the calculated strain was found to be 0.57 %.
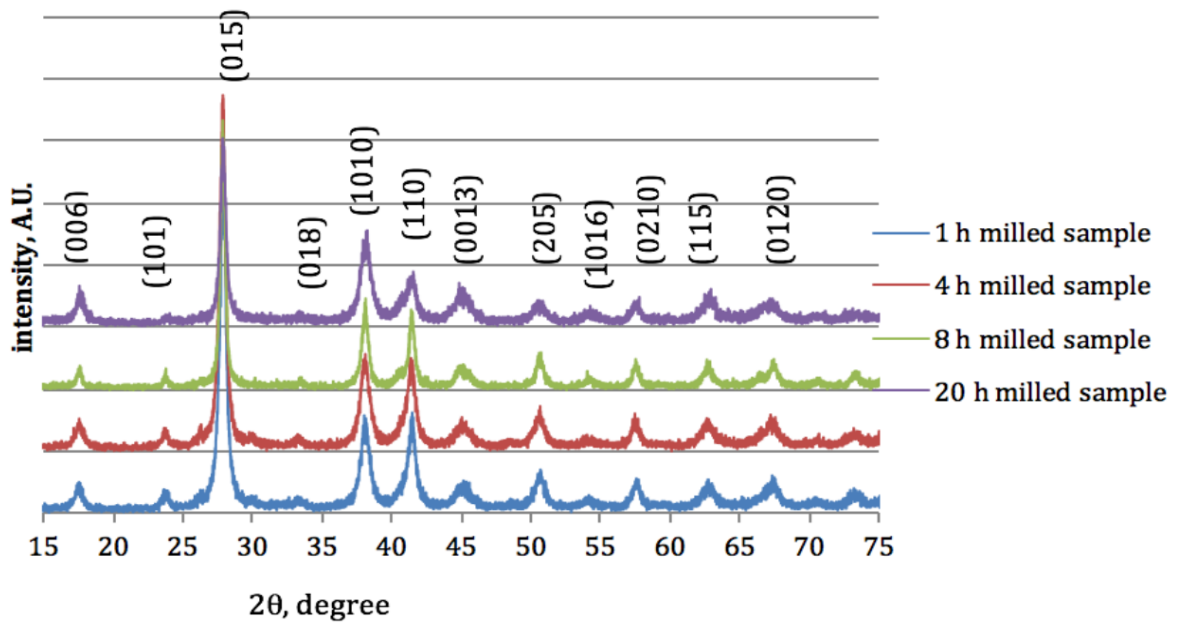
Figure 4.1: XRD patterns of as-milled n- type samples at different time of milling
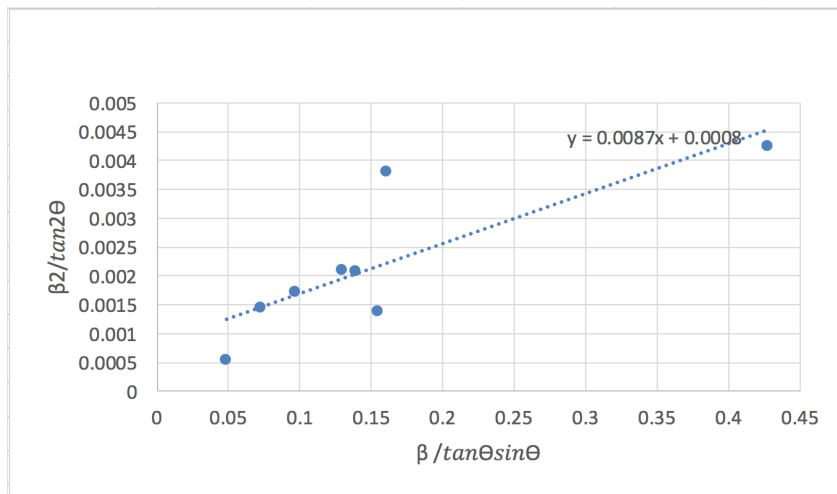
Figure 4.2: linear fit of Averbach method for as-milled n-type sample

This result shows that mechanical alloying technique has successfully synthesized nano-crystalline $Bi_2Te_{2.7}Se_{0.3}$ with grain size of 18 nm.

4.1.2   Structural morphology of n-type Bi-Te material

Scanning electron micrographs of as- milled n-type at different milling time 1, 4, 8 and 20 hours milling are shown in Figure 4.3. After 1 hour of milling, the particles of the as-milled materials appeared in large clusters as shown in Figure 4.3.a. As the milling time increases, the milled particles tend gradually to decrease as shown in Figure 4.3.b&c. Very fine particles in the range of 100 to 500 nm are produced after 20 hours of milling as can be seen in Figure 4.3.d. It is also shown that within each particle, there are several nano-features, which may correspond to the presence of nano-grains.The reduction of particle size with increasing the time of ball milling was also reported using SEM by Huayi Li et, al. [109].
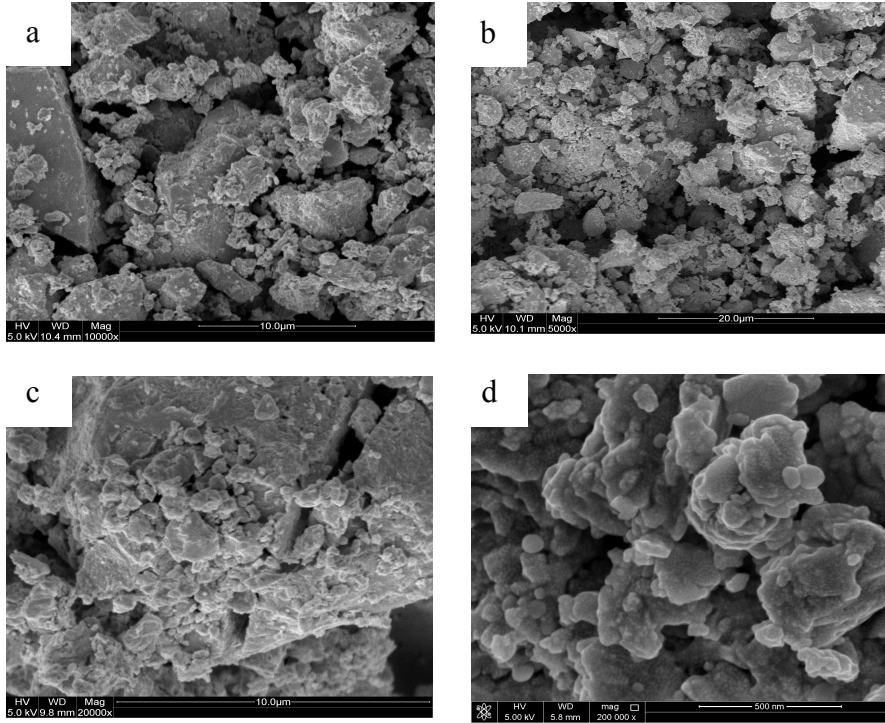
Figure 4.3: SEM image for as- milled n type, a) after 1 hour, b) 4 hours, c) 8hours, d) 20 hours

4.1.3 Transmission Electron Microscopy of n- type Bi-Te material

TEM was conducted on the as- milled n-type samples for further investigation of grain size. TEM bright and dark field images of the sample are illustrated in Figure 4.4 a & b. As can be seen, the grains of as- milled n- type Bi-Te are equiaxed with high angle grain boundaries and all grain size are below 50 nm. Statistical measurements of the grain size distribution for as- milled n-type based on a total grain count of 210 is shown in Figure 4.5,c. An important feature of the grain size distribution of the as- milled n-type nanostructure is that the grain size distribution is monotonic and lies within a very narrow

range. The average grain size value calculated from Figure 4.5 c is 21 nm. This grain size value is consistent with that determined from the XRD measurements (18 nm). Several researchers and scientists used mechanical alloying/ball milling to produce nano structured n-type and different grain sizes were obtained. For instance, L.D.Zhao et.al, [110] produced n-type sample by mechanical milling and obtained the material with fine grain size. The grain size for n-type material produced by Junyou Yang et.al, [89] was found to be in the micro-range. These results indicate that we have successfully produced our material in the nano-range with an average grain size of 21 nm. The challenge now is to maintain the grain size in the nano-range after hot compaction.
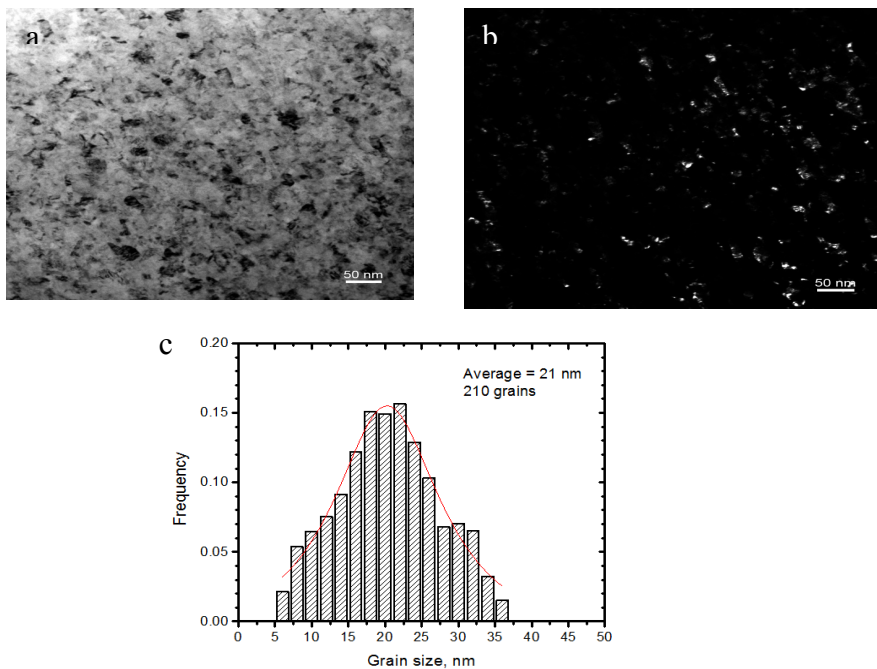
Figure 4.4: a) bright field image, b) dark field image, c) grain size distribution of as-milled n-type sample

4.2 Thermal behavior of n- type Bi-Te material

DSC scan was performed on the as- milled n-type sample in order to investigate the thermal behavior and stability of nano-grains. The heating process representing thermal behavior of as- milled n-type sample is shown in Figure 4.5. Due to the maximum temperature limitation of our Perkin Elmer DSC device, the sample was heated up to 410℃. Two exothermal peaks are appeared; the first exothermic peak is appeared at temperature of 315.5℃ and ended at 344.24℃ with ΔH = -0.465 J/g. This peak is relatively broad and shallow, which could be due to annihilation of defects, such as dislocations, during heating. The onset of the second exothermic peak appeared at 375.7℃ and ended at 394.96℃with ΔH = -2.14 J/g . This peak is relatively narrow and deep, which could be due to grain growth. This analysis allows us to select the suitable temperature for hot compaction in order to prevent grain growth. The hot compaction is performed at 300℃, which is quite far from the exothermic peaks. In order to investigate the influence of the hot compaction on the stability of phases and grain size, XRD analysis was performed on the hot compacted sample annealed at 300℃.
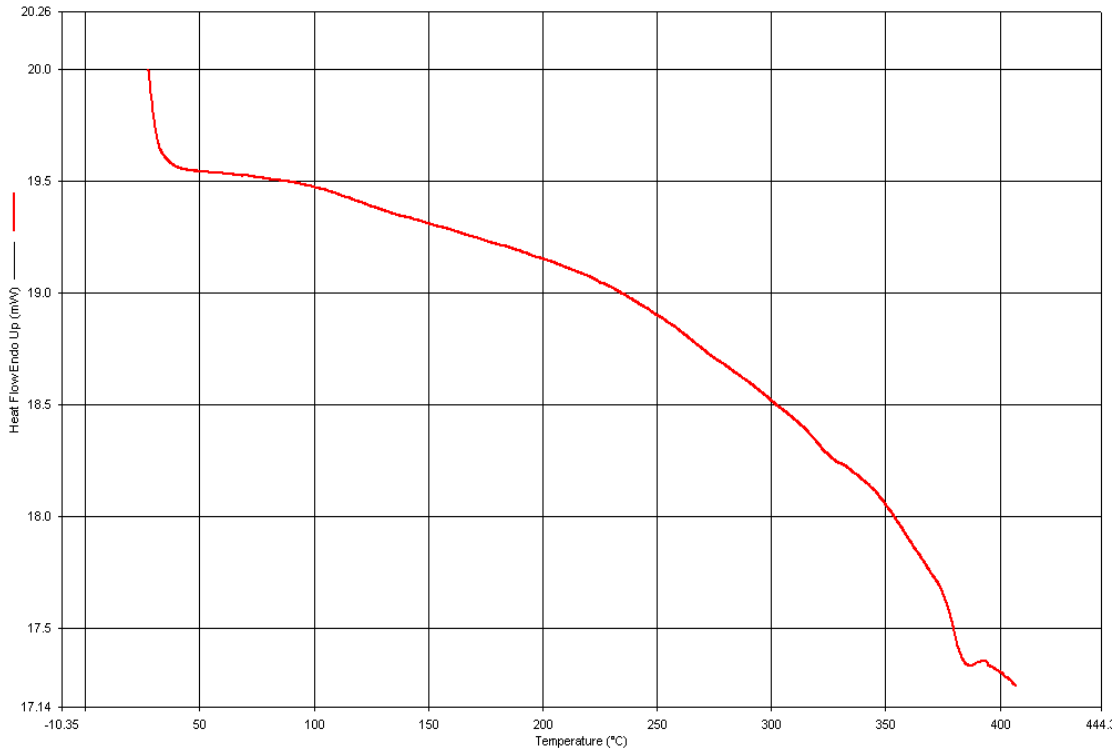
Figure 4.5: DSC analysis for milled n-type sample

The XRD pattern of the annealed sample compared to that pattern of the as- milled

sample is illustrated in Figure 4.6. The patterns for both samples are the same and can be

well indexed to the pattern of rohomohedral ($Bi_2Te_{2.7}Se_{0.3}$) single phase. For the annealed

sample, there are no extra peaks appeared which means that there are no extra phases

formed after annealing. The peaks are broadened indicating the fine grain structure of the

product. However, the peaks for annealed sample appeared to be little sharper than the as-

milled which could be due to relieving of strain resulting from the milling process or

grain growth. The calculations of grain size and lattice strain for the annealed sample

using Averbach method show that the strain is reduced by 50 % after annealing and the

average grain size grows from 18 nm to 21 nm which in total could explain the sharpness of XRD peaks for annealed sample.
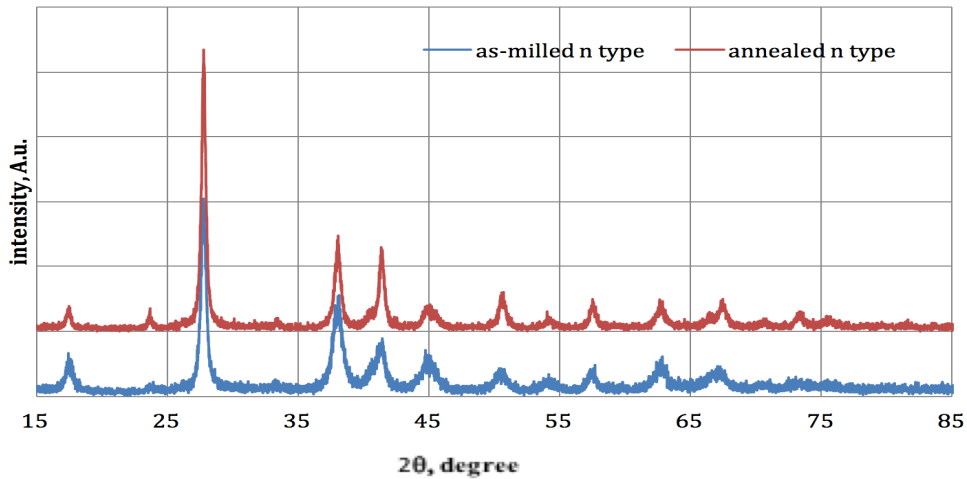
Figure 4.6: XRD pattern for as-milled and 300°C annealed n type sample

The values of grain size and lattice strain for as- milled and annealed samples are listed in Table 4.1. These results show that mechanical alloying technique with hot compaction under specific conditions have successfully synthesized nano-crystalline $Bi_2Te_{2.7}Se_{0.3}$ with grain size of 21 nm and there is no significant grain growth occurs after annealing.

Table 4. 1: Calculated grain size and lattice strain for as-milled and annealed n-type sample using Averbatch method

Sample type	Grain size (nm)	Starin (%)
As-milled n-type	18	0.571
Annealed n-type	21	0.282

4.3 Mechanical characterization results for n-type Bi-Te material

Vickers micro-hardness test was performed on the annealed n-type material at indentation load of 5 g load and dwelling time of 10 s. The average hardness results of the five readings for n- type sample is calculated to be 1.41± 0.01 GPa. Table 4.2 represents the hardness value of single crystal Bismuth Telluride and ingot n-type Bismuth Telluride compared to n-type material produced in this work. Comparison of these values shows significant enhancement in the hardness values for n-type sample produced in this work which is 1.41 GPa.

Table 4. 2: Hardness values for several BiTe materials compared to as-milled n- type in this work

Material	Hardness value (GPa)	Reference
Single crystal Bismuth telluride	0.6	[111]
Ingot n-type Bismuth telluride	o.65	[112]
n-type bismuth telluride (ball milled+sps)	1.1	[112]
This work (n-type Bismuth telluride)(as milled+ HP)	1.41(±0.01)	

This enhancement is attributed to the reduction in grain size where large area of grain boundaries can act as barriers to prevent dislocations motion. As the size of grains reduced, more grain boundaries are produced. Hence the hardness increases. This explains the increment of hardness of nano-structured compared to the single crystal and ingot materials where less grain boundaries are presented. However, for n-type Bismuth Telluride material

produced by Yu Pan et.al, [112] the value of hardness was reported to be 1.1 Gpa which is 59 % higher than the starting ingot and 21.4 % less than the hardness reported for n-type material in this work. The improvement in hardness from the ingot to nanostructured satisfied the fact that the reduction in grain size results in increasing the hardness of the material. The difference in hardness value between the n-type reported by Yu Pan et.al, and this work may contribute to the reduction of number of grain boundaries occurring as a result of grain growth in the first case compared to our case . Good mechanical properties give materials the ability to bear loads and improve reliability for applications [110], [112].

4.3 Thermoelectric transport property measurement for n-type Bi-Te material

The thermal conductivity of our nano-bulk n-type samples between 298 K and 373 K was measured in the same direction as the electrical resistivity and the Seebeck coefficient. The results of electrical resistivity, thermal conductivity, Seebeck coefficient and the calculated ZT value as a function of temperature are shown in Figure 4.7. The results reported from other research of crystalline ingot n-type bismuth telluride [112] and nano-grain sample made by mechanical milling and hot pressing [113], are included in Figure 4.7 for comparison purposes. From the graph, it is obvious that electrical resistivity is increasing with temperature for all samples. This is expected as increasing temperature will increase the charge carrier scattering. However, the highest resistivity value is reported for our sample which could be attributed to the high density of grain boundaries compared to other samples. The grain boundaries could affect the mobility of charge

carriers and hence increases the electrical resistivity. Thermal conductivity of our sample is the lowest among all other samples which could be contributed to small grain size obtained for our sample. The presence of grain boundaries increases the scattering of phonons, hence reduces lattice themal conductivity. The reduction in lattice thermal conductivity may also occur due to scattering at boundaries of the particles which can play as nanoinclusions and scatter mid to long wavelength as Kim [114] discussed. The Seebeck coefficient of our sample increases with increasing temperature and is higher than the other two samples. The high value of Seebeck coefficient is may due to the suppression of minority carriers at the grain boundaries which work as an energy filtering barriers [73].
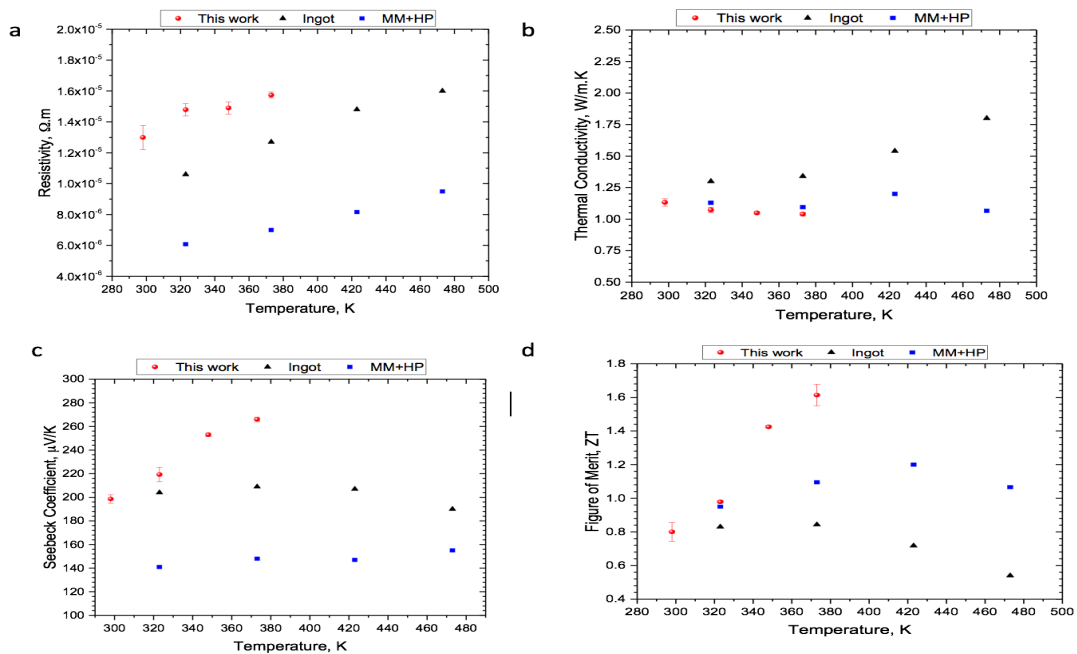
Figure 4.7: a) Electrical resistivity, b) thermal conductivity, c) Seebeck coefficient, d) figure of merit for as-milled hot pressed n-type material compared to the ingot and other MM+HP samples.

Figure 4.7.d shows ZT temperature dependence for all the samples. For our sample, ZT shows the highest value of 1.668 at 373 K. ZT value for our sample is the highest value reported for n-type bulk Bismuth telluride materials. It is even higher than ZT of single crystal bulk which is 1.54 and was considered as a higher value reported. However, our sample is prepared via a cost effective method rather than Bridgman method that was used to produce single crystal material. The enhancement of figure of merit for our sample is mainly due to optimization of preparation method and the suitable condition of that can tight the nano-powder and suppress the growth of grain boundaries.

CHAPTER 5

Results and discussion for p-type Bi-Te material

5.1 Structural characterization of p-type Bi-Te material

5.1.1 X-Ray diffractometer of p-type Bi-Te material

XRD patterns for as-milled p-type sample is shown in Figure 5.1. The pattern is well indexed to the pattern of rohomohedral Bi_2Te_3 single phase which indicate that ball milling can make elemental powder into single phase alloy. The peaks are broadened indicating the small grain size of the product.
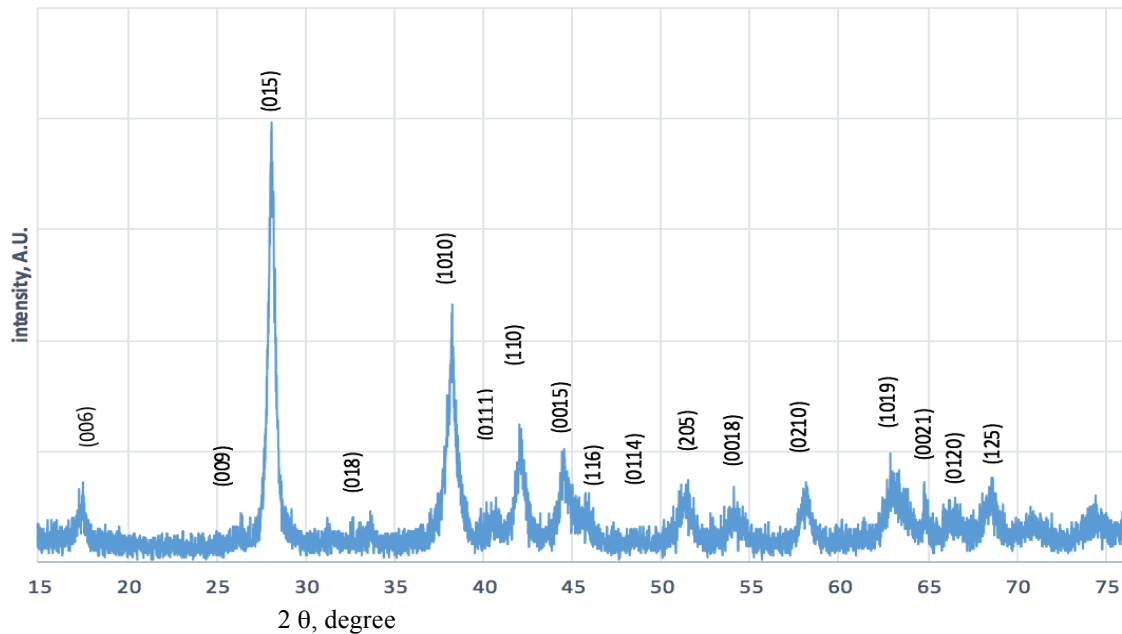
Figure 5.1: XRD pattern of as-milled p-type

Grain size with lattice strain were calculated using Averbach methods. A linear fitting of

$\frac{\beta 2}{tan2\theta}$ against $\frac{\beta}{tan\theta sin\theta}$ for all measured peaks of two samples was done. The slope of the

linear fitting was used to calculate the grain size whereas the intercept was used to calculate

the lattice strain. The calculated average grain size was found to be 29 nm whereas the

calculated lattice strain was found to be 0.45 %.
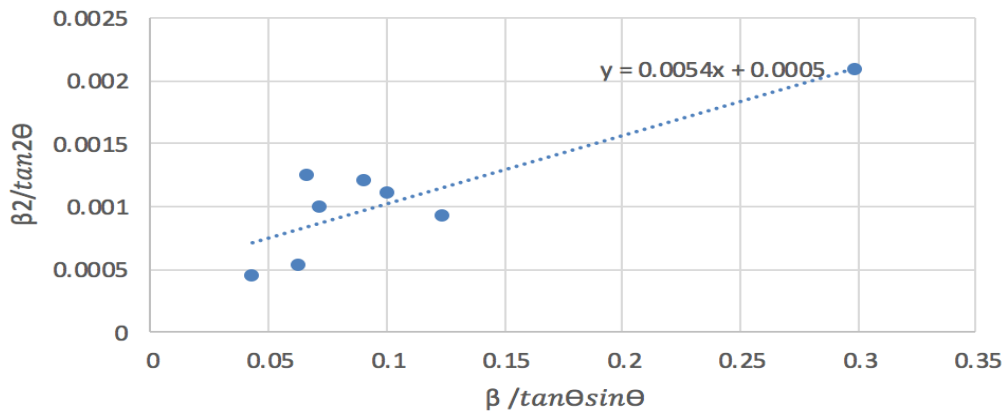
Figure 5.2: Linear fitting of Averbach method for as-milled p-type sample

5.1.2 Structural morphology of p-type Bi-Te material

Scanning electron micrographs of as- milled p-type at different magnification powers are

shown in Figure 5.3. The particles in Figure 5.3, a, the particles appeared to be

agglomerated in large clusters while the homogeneous shape of small particles is

obviously appeared in Figure 5.3 b and c. The size of powder particles is in the range of

100 to 500 nm. As can be seen within each particle, there are lots of nano-features which may correspond to the presence of nano-grains.
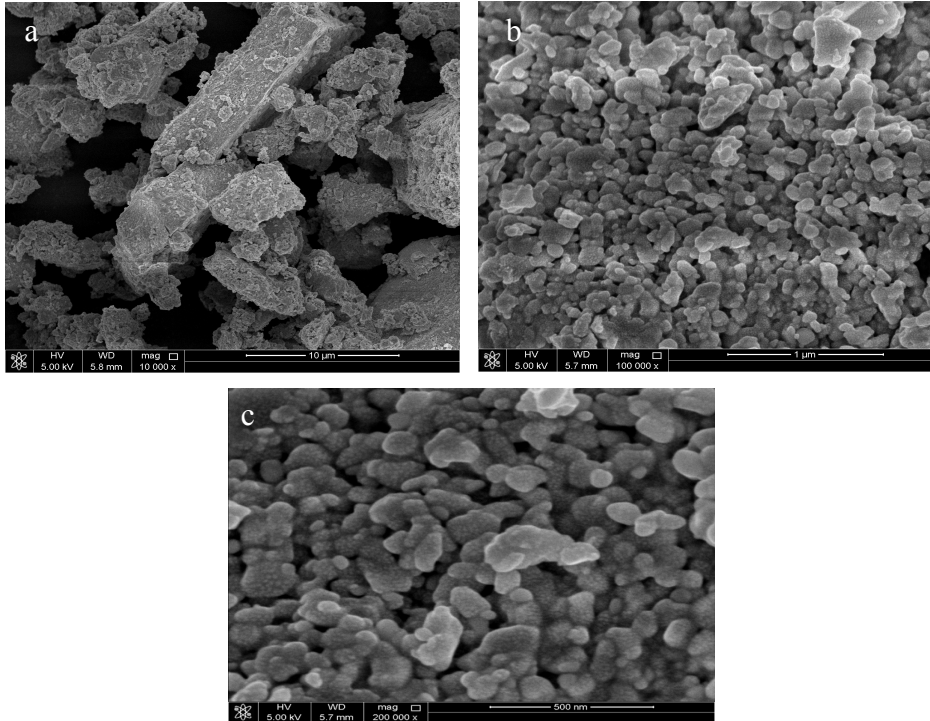
Figure 5.3: SEM for as-milled P-type bismuth telluride. a) 10,000 mag, b) 100,000 mag, c) 200,000 mag.

5.1.3 Transmission Electron Microscopy of p-type Bi-Te material

For further and precise investigation of the grain size and grain size distribution, TEM was conducted on as- milled p-type sample. Bright and dark field TEM images of the sample with TEM grain size distribution are presented in Figure 5.4 a, b and c. As can be

seen from Figure 5.4 a and b, the grains of as- milled p- type are equiaxed with high angle grain boundaries and all grain size are below 50 nm. For 190 grains, statistical measurements of the grain size distribution for as- milled p-type shows an average grain size of 19 nm as it is appeared in Figure 5.4,c. This grain size value shows a slight difference from the grain size determined from the XRD calculations which is 29 nm. However, TEM calculations is considered to be more accurate than XRD measurements. Similar to the grain size distribution obtained for as- milled n-type sample, the grain size distribution of as-milled p-type, as in the case of n-type material, lies within a very narrow range. Several groups who prepared the same materials by the same preparation method, used the same calculations of grain size [73], [85], [115]. For instance, Yi Ma et.al [73] reported the value of average grain size for as-milled p-type material to be 10 nm. However, after hot pressing the grains grow up to more than 50 nm. Thus, the main goal in our case is to try keeping the grain size after compaction in the nano-range.
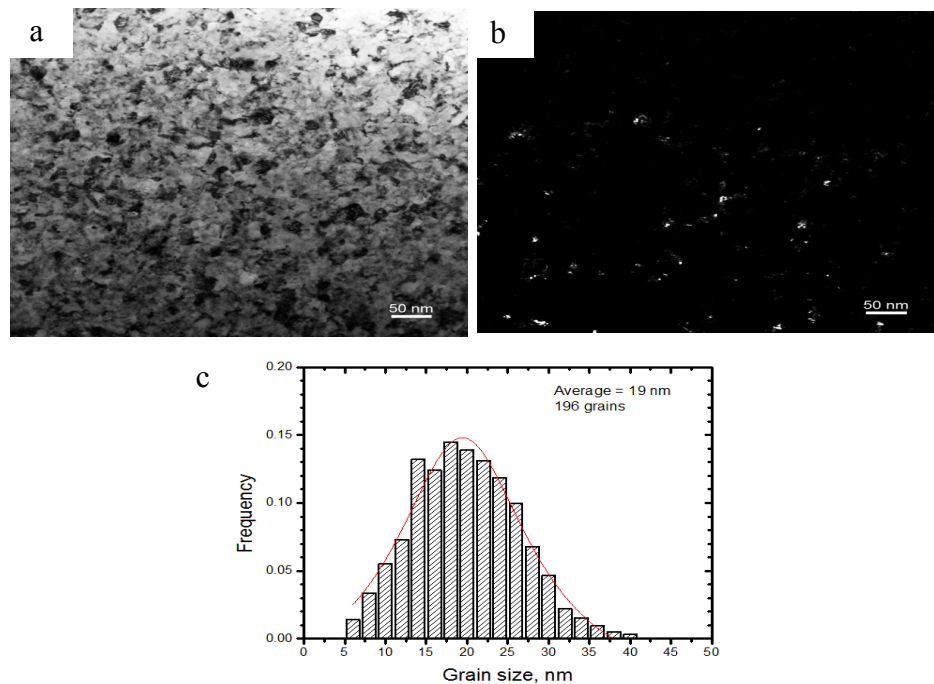
Figure 5.4: a) bright field TEM image, b) dark field TEM image for as-milled p-type sample, c) TEM grain size distribution.

5.2 Thermal behavior of p-type Bi-Te material

In order to study the thermal behavior and stability of nano-grains, DSC scan was performed on the as- milled p-type sample. Figure 5.5 represents thermal behavior of as-milled p-type sample during the heating process from room temperature up to 430°C. An endothermic peak is observed at 420°C matching with the melting point of the material. An exothermic peak is appeared at onset temperature of 265. 5°Cand ended at 286.4°C with ΔH = -1.89 J/g. This could be due to recovery which is due to annihilation and recombination of dislocations to form cells and sub-grains. Recovery occurs usually at

low temperature and result in releasing energy [116] . XRD analysis was performed on the annealed p-type sample in order to investigate the effect of annealing on the grain size and stability of phases. Figure 5.6 shows the XRD patterns of annealed sample compared to that of the as- milled sample. As can be shown, similar peaks to that of rohomohedral BiTe phase were obtained after annealing with no extra peaks. This result means that there are no new phases formed after annealing. The peaks of the annealed sample are broadened similar to that obtained for the as-milled sample but with little sharpness. The sharpness of the peaks could be contributed to the relieving some of the strain occurring during the milling process or to the grain growth. For further justifications, Averbach calculations were used to calculate the lattice strain and the average grain size after annealing process. The average grain size was calculated to be 38 nm and the calculated strain shows a reduction by 69 % compared to the as-milled sample.
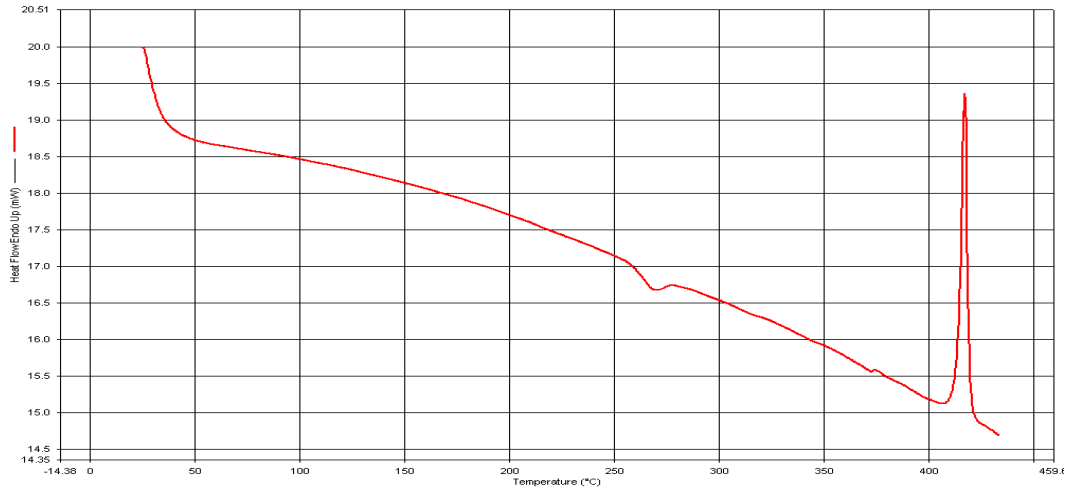
Figure 5.5: DSC analysis for as-milled p-type sample
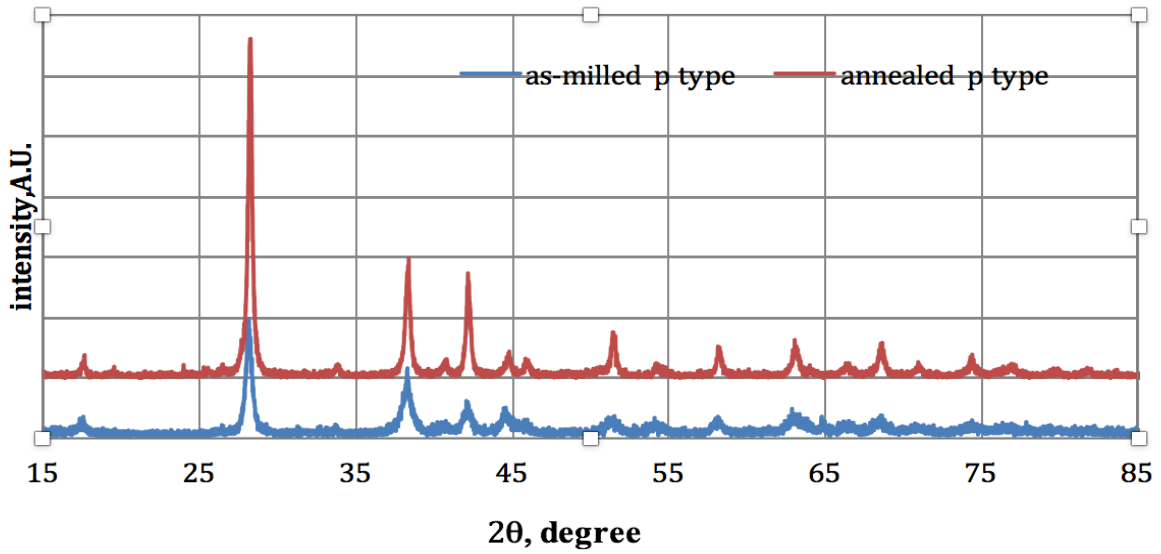
Figure 5.6: XRD patterns for as-milled and annealed p-type sample

The values of grain size and lattice strain for as- milled and annealed sample are listed in Table 5.1. Although these results show slide growth in the average grain size after annealing but mechanical alloying technique with hot compaction under specific conditions is considered to be a successful synthesized technique to produce nano-crystalline $Bi_{0.4}Sb_{1.6}Te_3$.

Table 5. 1: Calculated grain size and lattice strain for as-milled and annealed p-type using Averbach method

Sample type	Grain size (nm)	Starin (%)
As-milled p-type	28	0.45
Annealed p-type	38	0.14

5.3 Mechanical characterization results for p-type Bi-Te material

Vickers micro-hardness test at indentation load of 5 g and dwelling time of 10 s was performed on the annealed p-type sample. Five readings of hardness value at different places on the sample surface were taken. The average hardness value was calculated to be 1.39 GPa. Comparison between the hardness value of single crystal Bismuth Telluride, ingot p-type Bismuth Telluride, ball milled and sps p-type bismuth telluride with as-milled and hot pressed p-type sample produced in this work are listed in Table 5.2. Significant enhancement is obtained for the hardness values of as- milled sample produced in this work which is 1.39 ± 0.005 % GPa.

Table 5. 2: Hardness values for several BiTe compared to as- milled p-type in this work

Material	Hardness value (GPa)	Reference
Single crystal Bismuth telluride	0.6	[111]
Ingot P-type bismuth telluride	0.57	[112]
P-type bismuth telluride(ball milled+sps)	0.94	[112]
This work (P-type Bismuth telluride)	1.39 (± 0.005)	

As mentioned for the hardness enhancement in n-type material, the enhancement in p type could also attributed to the reduction in grain size. The grain boundaries that are produced during milling process can act as barriers to prevent dislocations motion. As a result, increasing the number of grain boundaries result in increasing the hardness value. This gives us a logical reason for the increment of hardness of nano-structured compared to the

single crystal and ingot material where less grain boundaries are presented. However, for p-type Bismuth Telluride material produced by Yu Pan et.al, [112] the value of hardness was reported to be 0.94 Gpa, which is 40 % higher than the starting ingot and 30 % less than the hardness reported for p-type material in this work. The enhancement in the hardness value for p-type sample produced in this work compared to the p-type reported by Yu Pan et.al, may be attributed to the ability of keeping large number of grain boundaries by keeping the material in the nano-range. Figure 4.8 represents a graph of hardness values of several n-type materials and p-type materials using the hardness value of single crystal Bismuth telluride as a reference. The enhancement of hardness value for nano-crystalline p- and n-type is obvious compared to the single crystal and ingot materials which proves that the grain size is reduced.
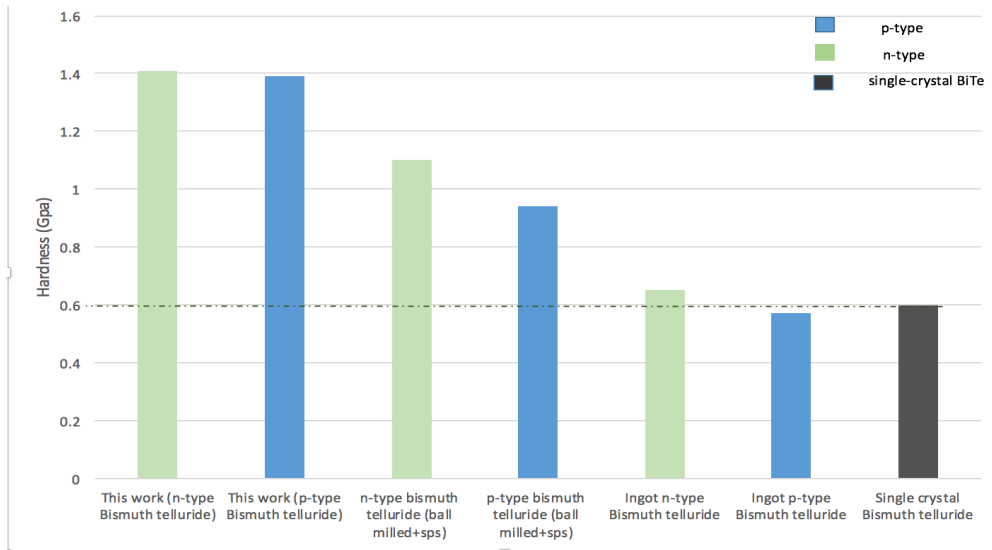
Figure 5.7: Graph representing hardness values of several n-type materials, p-type materials compared to single crystal BiTe material as a reference

5.4 Thermoelectric transport property measurement for p-type

Thermoelectric properties (thermal resistivity, thermal conductivity, Seebeck coefficient) of our nano-bulk p- type samples were measured in the same direction between 298 k and 373 K. All the results of thermoelectric properties with ZT as a function of temperature are shown in Figure 5.8. For comparison purposes, other reported results of crystalline ingot p-type [112] and as-milled hot pressed nano-grain sample made from elemental chunks [73] are included in the graphs. It is obvious from Figure 5.8,a that electrical resistivity of all samples increases with temperature. Since increasing temperature increases the scattering of charge carriers, this will increase the resistivity. Figure 5.8,b

shows that thermal conductivity of our sample is low and lower than that of ingot

material which is expected because of scattering of phonons at grain boundaries as well

as scattering at boundaries of the particles. The value of thermal conductivity is below 1.6

W/mK for our sample which is desired for best thermoelectric materials [73]. The highest

Seebeck coefficient among all the samples is reported for our sample as shown in Figure

5.8,c. The highest Seebeck coefficient value indicates that the grain boundaries act as

energy filtering barriers that suppress the minority carriers with low energy [73]. The

positive value of Seebeck coefficient indicates that the tested sample is p-type. Figure

5.8,d shows the temperature dependence of ZT for all the samples. The ZT value of our

sample shows the highest value of 1.78 at 373 K which is higher than the value of ZT of

all other samples. The ZT value of 1.78 is comparable to the highest ZT value reported

for p-type single crystal which is 1.88. However, the preparing method used in our case is

simple and cost effective rather than method followed to prepare single crystals. The

improvement in ZT value compared to other samples is contributed to the preparation and

compaction methods that result in producing and keeping the material in the nano-range.
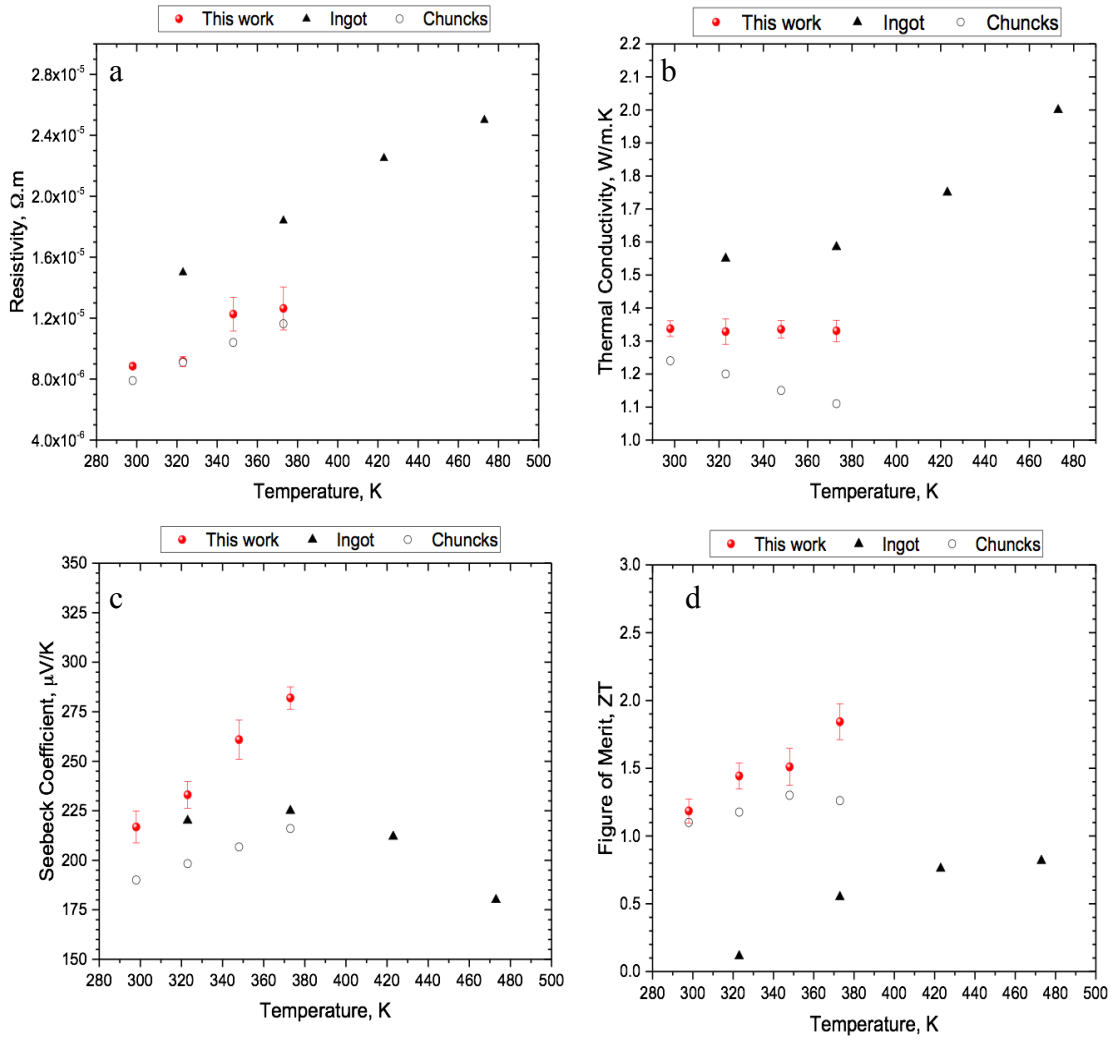
Figure 5.8: a) Electrical resistivity, b) thermal conductivity), c) seebek coefficient,d) figure of merit of as-milled, hot pressed, p-type sample

CONCLUSION

In conclusion, we have successfully synthesized n-type ($Bi_2Te_{2.7}Se_{0.3}$) and p-type ($Bi_{0.4}Sb_{1.6}Te_3$) nano-crystalline bulk thermoelectric materials materials from elemental powders. Mechanical alloying with optimum conditions of hot pressing (up to 300^0C) were used to produce the materials. Preparing the materials from elemental powders is a simple, environmentally friendly compared to preparing the materials from crystalline ingot since the energy used for preparing the ingot is conserved in our case. The thesis conclusion remarks are:

- The average grain size value of the as-milled n- and p-type was found to be 21 nm and 19 nm, respectively.

- The average gain size of the as-milled, hot compacted final product of n- and p-type was found to be 21 nm and 38 nm, respectively.

- Hardness measurements for both samples show a significant enhancement to 1.39 ± 0.005 GPa for p-type and 1.41 ± 0.01 Gpa for n-type compared to 0.6 GPa for single crystal Bismuth Telluride material.

- Seebeck coefficient for both p-type and n-type show an enhancement compared to other materials produced with the same technique.

- Both materials achieve significant reduction of thermal conductivity which is mainly due to scattering of phonons at grain boundaries produced by nano-structuring.

- Significant improvement in ZT was achieved for both p-type and n-type materials compared to the state of art materials. ZT increases with increasing temperature and give the maximum value at 373 k with 1.78 for p-type and 1.668 for n-type.

- The improvement in ZT is attributed to the nanostructure that reduces lattice thermal conductivity by increasing phonon scattering and enhance Seebeck coefficient by energy filtering of low energy carriers.

REFERENCES

[1] H. Alam and S. Ramakrishna, "A review on the enhancement of figure of merit from bulk to nano-thermoelectric materials," *Nano Energy*. 2013.

[2] X. Zhang and L.-D. Zhao, "Thermoelectric materials: energy conversion between heat and electricity," *J. Mater.*, vol. 1, no. 2, pp. 92–105, 2015.

[3] X. W. Wang, H. Lee, Y. C. Lan, G. H. Zhu, G. Joshi, D. Z. Wang, J. Yang, a. J. Muto, M. Y. Tang, J. Klatsky, S. Song, M. S. Dresselhaus, G. Chen, and Z. F. Ren, "Enhanced thermoelectric figure of merit in nanostructured n-type silicon germanium bulk alloy," *Appl. Phys. Lett.*, vol. 93, no. 19, p. 193121, 2008.

[4] Z. G. Chen, G. Hana, L. Yanga, L. Cheng, and J. Zou, "Nanostructured thermoelectric materials: Current research and future challenge," *Progress in Natural Science: Materials International*, vol. 22, no. 6. pp. 535–549, 2012.

[5] M. S. Dresselhaus, G. Chen, M. Y. Tang, R. Yang, H. Lee, D. Wang, Z. Ren, J. P. Fleurial, and P. Gogna, "New directions for low-dimensional thermoelectric materials," *Adv. Mater.*, vol. 19, no. 8, pp. 1043–1053, 2007.

[6] R. Venkatasubramanian, E. Siivola, T. Colpitts, and B. O'Quinn, "Thin-film thermoelectric devices with high room-temperature figures of merit.," *Nature*, vol. 413, no. 6856, pp. 597–602, 2001.

[7] W. Xie, X. Tang, Y. Yan, Q. Zhang, and T. M. Tritt, "High thermoelectric performance BiSbTe alloy with unique low-dimensional structure," *J. Appl. Phys.*, vol. 105, no. 11, 2009.

[8]   Z. Li, G. L. Zhao, P. Zhang, S. Guo, and J. Tang, "Thermoelectric Performance of Micro/Nano-Structured Bismuth-Antimony-Telluride Bulk from Low Cost Mechanical Alloying," *Mater. Sci. Appl.*, vol. 3, pp. 833–837, 2012.

[9]   V. Viswanathan, T. Laha, K. Balani, A. Agarwal, and S. Seal, "Challenges and advances in nanocomposite processing techniques," *Mater. Sci. Eng. R Reports*, vol. 54, no. 5–6, pp. 121–285, 2006.

[10]   W. Dissanayaka Wijesooriyage, "Electrochemical Deposition and Characterization of Thermoelectric Thin Films of (Bi x Sb 1-x) 2 Te 3," 2011.

[11]   J. Yang, L. Xi, W. Qiu, L. Wu, X. Shi, L. Chen, J. Yang, W. Zhang, C. Uher, and D. J. Singh, "On the tuning of electrical and thermal transport in thermoelectrics: an integrated theory–experiment perspective," *npj Comput. Mater.*, vol. 2, no. October 2015, p. 15015, 2016.

[12]   M. Hamid Elsheikh, D. A. Shnawah, M. F. M. Sabri, S. B. M. Said, M. Haji Hassan, M. B. Ali Bashir, and M. Mohamad, "A review on thermoelectric renewable energy: Principle parameters that affect their performance," *Renewable and Sustainable Energy Reviews*. 2014.

[13]   A. Mehdizadeh Dehkordi, M. Zebarjadi, J. He, and T. M. Tritt, "Thermoelectric power factor: Enhancement mechanisms and strategies for higher performance thermoelectric materials," *Materials Science and Engineering R: Reports*. 2015.

[14]   P. Pichanusakorn and P. Bandaru, "Nanostructured thermoelectrics," *Materials Science and Engineering R: Reports*, vol. 67, no. 2–4. pp. 19–63, 2010.

[15]   W. He, G. Zhang, X. Zhang, J. Ji, G. Li, and X. Zhao, "Recent development and

application of thermoelectric generator and cooler," *Appl. Energy*, vol. 143, pp. 1–25, 2015.

[16] M. Hamid Elsheikh, D. A. Shnawah, M. F. M. Sabri, S. B. M. Said, M. Haji Hassan, M. B. Ali Bashir, and M. Mohamad, "A review on thermoelectric renewable energy: Principle parameters that affect their performance," *Renewable and Sustainable Energy Reviews*, vol. 30. pp. 337–355, 2014.

[17] P. Martín-González, Marisol Caballero-Calero, O. Díaz-Chao, "Nanoengineering thermoelectrics for 21st century: Energy harvesting and other trends in the field," *Renew. Sustain. Energy Rev.*, vol. 24, pp. 288–305, 2013.

[18] T. M. Tritt and M. a. Subramanian, "Thermoelectric Materials, Phenomena, and Applications: A Bird's Eye View," *MRS Bull.*, vol. 31, no. March, pp. 188–198, 2006.

[19] B. . Peter D. Heinz, "First principle study of thermoelectric properties of Zinc-Oxide nanowires," 2010.

[20] A. Kadhim, A. Hmood, H. A. Hassan, and D. D. Sarma, "Thermoelectric generation device based on p-type Bi 0.4 Sb 1.6 Te 3 and n-type Bi 2 Se 0.6 Te 2.4 bulk materials prepared by solid state microwave synthesis," *Solid State Commun.*, vol. 166, pp. 44–49, 2013.

[21] H. Alam and S. Ramakrishna, "A review on the enhancement of figure of merit from bulk to nano-thermoelectric materials," *Nano Energy*, vol. 2, no. 2. pp. 190–212, 2013.

[22] K. S. Bhargavi and S. S. Kubakaddi, "Scattering mechanisms and diffusion

thermopower in a bilayer graphene," *Phys. E Low-Dimensional Syst. Nanostructures*, vol. 52, pp. 116–121, 2013.

[23]   R. Prozorov, "Conductors, Semiconductors, Superconductors: An Introduction to Solid State Physics," *Phys. Today*, vol. 68, no. 5, pp. 52–52, 2015.

[24]   K. D. Belashchenko and D. V Livanov, "Phonon effects in the thermoelectric power of impure metals," *J. Phys. Condens. Matter*, vol. 10, p. 7553, 1998.

[25]   S. Bathula, M. Jayasimhadri, N. Singh, A. K. Srivastava, J. Pulikkotil, A. Dhar, and R. C. Budhani, "Enhanced thermoelectric figure-of-merit in spark plasma sintered nanostructured n-type SiGe alloys," *Appl. Phys. Lett.*, vol. 101, no. 21, 2012.

[26]   G. G. Lee and G. H. Ha, "Fabrication of the Bi0.5Sb1.5Te3 thermoelectric material by fusion-mechanical milling and spark plasma sintering," *Adv. Powder Technol.*, vol. 26, no. 1, pp. 208–212, 2015.

[27]   T. M. Tritt, *Thermal Conductivity: Theory, Properties, and Applications*, vol. 53. 2004.

[28]   G. J. Snyder and E. S. Toberer, "Complex thermoelectric materials," *Nat. Mater.*, vol. 7, no. 2, pp. 105–114, 2008.

[29]   R. Yang and G. Chen, "Nanostructured thermoelectric materials: from superlattices to nanocomposites," *Mater. Integr.*, vol. 18, pp. 31–36, 2005.

[30]   Z. Tian, S. Lee, and G. Chen, "A Comprehensive Review of Heat Transfer in Thermoelectric Materials and Devices," *Annu. Rev. Heat Transf.*, pp. 1–64, 2014.

[31]   L. D. Hicks and M. S. Dresselhaus, "Effect of quantum-well structures on the

thermoelectric figure of merit," *Physical Review B*, vol. 47. pp. 12727–12731, 1993.

[32] L. D. Hicks, T. C. Harman, and M. S. Dresselhaus, "Use of quantum-well superlattices to obtain a high figure of merit from nonconventional thermoelectric materials," *Appl. Phys. Lett.*, vol. 63, no. 23, pp. 3230–3232, 1993.

[33] A. a Balandin, "Nanophononics: phonon engineering in nanostructures and nanodevices.," *J. Nanosci. Nanotechnol.*, vol. 5, pp. 1015–1022, 2005.

[34] A. A. Balandin and D. L. Nika, "Phononics in low-dimensional materials," *Materials Today*, vol. 15, no. 6. pp. 266–275, 2012.

[35] S. K. Bux, J.-P. Fleurial, and R. B. Kaner, "Nanostructured materials for thermoelectric applications.," *Chem. Commun. (Camb).*, vol. 46, no. 44, pp. 8311–8324, 2010.

[36] W. Liu, X. Yan, G. Chen, and Z. Ren, "Recent advances in thermoelectric nanocomposites," *Nano Energy*, vol. 1, no. 1, pp. 42–56, 2012.

[37] J. R. Szczech, J. M. Higgins, and S. Jin, "Enhancement of the thermoelectric properties in nanoscale and nanostructured materials," *J. Mater. Chem.*, vol. 21, no. 12, p. 4037, 2011.

[38] A. Wrona, K. Bilewska, J. Mazur, M. Lis, and M. Staszewski, "Properties of thermoelectric Zn-Sb type material directly synthesized by spark plasma sintering," *J. Alloys Compd.*, 2014.

[39] C. Wan, Y. Wang, N. Wang, W. Norimatsu, M. Kusunoki, and K. Koumoto, "Development of novel thermoelectric materials by reduction of lattice thermal

conductivity," *Sci . Technol . Adv . Mater . 11 044306 Sci . Technol . Adv . Mater*, vol. 11, pp. 44306–7, 2010.

[40] A. Soni, Y. Shen, M. Yin, Y. Zhao, L. Yu, X. Hu, Z. Dong, K. A. Khor, M. S. Dresselhaus, and Q. Xiong, "Interface driven energy filtering of thermoelectric power in spark plasma sintered Bi 2Te 2.7Se 0.3 nanoplatelet composites," *Nano Lett.*, vol. 12, no. 8, pp. 4305–4310, 2012.

[41] D. M. Rowe, "Thermoelectrics handbook: macro to nano," *Thermoelectrics Handbook Macro to Nano*, vol. 80, no. 10. p. 1014, 2005.

[42] S. Lwe and L. Weera, "Analytical Performance Evaluation of Thermoelectric Modules Using Effective Material Properties," 2014.

[43] A. Shakouri and J. Baskin, "Recent Developments in Semiconductor Thermoelectric Physics and Materials," *Annu. Rev. Mater. Res*, vol. 41, pp. 399–431, 2011.

[44] S. B. Riffat and X. Ma, "Thermoelectrics: A review of present and potential applications," *Applied Thermal Engineering*, vol. 23, no. 8. pp. 913–935, 2003.

[45] D. M. Rowe, "CRC Handbook of Thermoelectrics," *New York*, vol. 16, no. 1–4. pp. 1251–1256, 1995.

[46] G. R. Joshi, "Study of Thermoelectric Properties of Sb , and Half-Heusler Bulk Materials," 2010.

[47] A. Mishra, S. Bhattacharjee, and S. Anwar, "Simple apparatus to measure Seebeck coefficient up to 900 K," *Meas. J. Int. Meas. Confed.*, vol. 68, pp. 295–301, 2015.

[48] T. Road, S. Maharashtra, and U. Shivaji, "A REVIEW OF RECENT

DEVELOPMENTS IN MATERIALS AND APPLICATIONS OF

NANOTHERMOELECTRIC MATERIALS," *Mech. Eng.*, 2007.

[49]   D. Zhao and G. Tan, "A review of thermoelectric cooling: Materials, modeling and

applications," *Applied Thermal Engineering*. 2014.

[50]   J. Zheng, "Recent advances on thermoelectric materials," *Front. Phys. China*, vol.

3, no. 3, pp. 269–279, 2008.

[51]   H. Kleinke, "New bulk materials for thermoelectric power generation: clathrates

and complex antimonides," *Chem. Mater.*, vol. 22, no. 3, pp. 604–611, 2010.

[52]   J. Yang, H.-L. Yip, and A. K.-Y. Jen, "Rational Design of Advanced

Thermoelectric Materials," *Adv. Energy Mater.*, no. 2, p. n/a–n/a, 2013.

[53]   G. Geng Kirill Kovnir, "'Filled Skutterudite Nanocomposites': A Proposal for a

New Class of Thermoelectric Materials and Theoretical & Computational Analysis

of a Hypothetical Example."

[54]   D. L. Medlin and G. J. Snyder, "Interfaces in bulk thermoelectric materials A

review for Current Opinion in Colloid and Interface Science," *Curr. Opin. Colloid

Interface Sci.*, vol. 14, pp. 226–235, 2009.

[55]   L. Shi, P. S. Ho, J. R. Howell, S. K. Banerjee, and Z. Yao, "Thermal and

Thermoelectric Transport Measurements of One-Dimensional Nanostructures."

[56]   P. Puneet, R. Podila, M. Karakaya, S. Zhu, J. He, T. M. Tritt, M. S. Dresselhaus,

and A. M. Rao, "Preferential scattering by interfacial charged defects for enhanced

thermoelectric performance in few-layered n-type Bi2Te3.," *Sci. Rep.*, vol. 3, p.

3212, 2013.

[57] M. Keshavarz Khorasgani, "Synthesis and characterization of bismuth telluride-based nanostructured thermoelectric comosite materials," 2014.

[58] P. Vaqueiro and A. V. Powell, "Recent developments in nanostructured materials for high-performance thermoelectrics," *J. Mater. Chem.*, vol. 20, no. 43, p. 9577, 2010.

[59] M. S. Dresselhaus, G. Dresselhaus, X. Sun, Z. Zhang, S. B. Cronin, and T. Koga, "Low Dimensional Thermoelectric Materials," *Физика твердого тела*, vol. 41, no. 5, 1999.

[60] J. Zhou, C. Jin, J. H. Seol, X. Li, and L. Shi, "Thermoelectric properties of individual electrodeposited bismuth telluride nanowires," *Appl. Phys. Lett.*, vol. 87, no. 13, pp. 1–3, 2005.

[61] G. Zhang, B. Kirk, L. a Jauregui, H. Yang, X. Xu, Y. P. Chen, and Y. Wu, "Rational synthesis of ultrathin n-type Bi2Te3 nanowires with enhanced thermoelectric properties.," *Nano Lett.*, vol. 12, no. 1, pp. 56–60, 2012.

[62] M. K. KHORASGANI, "Synthesis and characterization of semiconductor nanomaterials for thermoelectric applications," 2014.

[63] J. R. Sootsman, D. Y. Chung, and M. G. Kanatzidis, "New and old concepts in thermoelectric materials," *Angewandte Chemie - International Edition*. 2009.

[64] K. F. Hsu, S. Loo, F. Guo, W. Chen, J. S. Dyck, C. Uher, T. Hogan, E. K. Polychroniadis, and M. G. Kanatzidis, "Cubic AgPbmSbTe2+ m: Bulk thermoelectric materials with high figure of merit," *Science (80-.).*, vol. 303, no. 5659, pp. 818–821, 2004.

[65] G. Joshi, H. Lee, Y. Lan, X. Wang, G. Zhu, D. Wang, R. W. Gould, D. C. Cuff, M. Y. Tang, M. S. Dresselhaus, G. Chen, and Z. Ren, "Enhanced thermoelectric figure-of-merit in nanostructured p-type silicon germanium bulk alloys," *Nano Lett.*, vol. 8, no. 12, pp. 4670–4674, 2008.

[66] Y. Lan, A. J. Minnich, G. Chen, and Z. Ren, "Enhancement of thermoelectric figure-of-merit by a bulk nanostructuring approach," *Adv. Funct. Mater.*, vol. 20, no. 3, pp. 357–376, 2010.

[67] M. Saleemi, M. S. Toprak, S. Li, M. Johnsson, and M. Muhammed, "Synthesis, processing, and thermoelectric properties of bulk nanostructured bismuth telluride (Bi2Te3)," *J. Mater. Chem.*, vol. 22, p. 725, 2012.

[68] X. Tang, W. Xie, H. Li, W. Zhao, Q. Zhang, and M. Niino, "Preparation and thermoelectric transport properties of high-performance p-type Bi2Te3 with layered nanostructure," *Appl. Phys. Lett.*, vol. 90, no. 1, 2007.

[69] X. B. Zhao, X. H. Ji, Y. H. Zhang, T. J. Zhu, J. P. Tu, and X. B. Zhang, "Bismuth telluride nanotubes and the effects on the thermoelectric properties of nanotube-containing nanocomposites," *Appl. Phys. Lett.*, vol. 86, no. 6, pp. 1–3, 2005.

[70] C. L. Chen, Y. Y. Chen, S. J. Lin, J. C. Ho, P. C. Lee, C. D. Chen, and S. R. Harutyunyan, "Fabrication and characterization of electrodeposited bismuth telluride films and nanowires," *J. Phys. Chem. C*, vol. 114, no. 8, pp. 3385–3389, 2010.

[71] W. Xie, S. Wang, S. Zhu, J. He, X. Tang, Q. Zhang, and T. M. Tritt, "High performance Bi2Te3 nanocomposites prepared by single-element-melt-spinning

spark-plasma sintering," *J. Mater. Sci.*, vol. 48, no. 7, pp. 2745–2760, 2013.

[72]   J. P. Carmo, L. M. Gonçalves, and J. H. Correia, "Micro and nanodevices for thermoelectric converters," *Scanning Probe Microsc. Nanosci. Nanotechnol. 2*, no. 1, 2011.

[73]   Y. Ma, Q. Hao, B. Poudel, Y. Lan, B. Yu, D. Wang, G. Chen, and Z. Ren, "Enhanced thermoelectric figure-of-merit in p-type nanostructured bismuth antimony tellurium alloys made from elemental chunks," *Nano Lett.*, vol. 8, no. 8, pp. 2580–2584, 2008.

[74]   X. Ji and T. M. Tritt, "Solution Chemical Synthesis of nanostructured Thermoelectric Materials Solution Chemical Synthesis of nanostructured Thermoelectric Materials," *J. South Carolina Acad. Sci.*, vol. 6, no. 2, 2008.

[75]   S. Gupta, S. Neeleshwar, V. Kumar, and Y. Y. Chen, "Synthesis of bismuth telluride nanostructures by refluxing method," *Adv. Mater. Lett.*, vol. 3, no. 1, pp. 50–54, 2012.

[76]   Y. Zhang, H. Wang, S. Kräemer, Y. Shi, F. Zhang, M. Snedaker, K. Ding, M. Moskovits, G. J. Snyder, and G. D. Stucky, "Surfactant-Free Synthesis of Bi 2 Te 3 −Te Micro−Nano Heterostructure with Enhanced Thermoelectric Figure of Merit," *ACS Nano*, vol. 5, no. 4, pp. 3158–3165, 2011.

[77]   E. Alleno, S. Bastide, and C. Godart, "Bi 2 Se 3 nanocrystalline powders synthesized in solution from H 2 Se electrochemically generated in-situ P2-21-1 P2-21-2," pp. 1–4, 1990.

[78]   L. Yang, Z. G. Chen, M. Hong, G. Han, and J. Zou, "Enhanced Thermoelectric

Performance of Nanostructured Bi2Te3 through Significant Phonon Scattering," *ACS Appl. Mater. Interfaces*, vol. 7, no. 42, pp. 23694–23699, 2015.

[79]   G. Nolas, M. R. Dirmyer, J. Martin, G. S. Nolas, A. Sen, and J. V Badding, "Thermal and Electrical Conductivity of Size- Tuned Bismuth Telluride Nanoparticles Thermal and Electrical Conductivity of Size-Tuned Bismuth Telluride Nanoparticles," *interScience*, no. April, pp. 933–937, 2009.

[80]   H. Boettner, D. Ebling, A. Jacquot, U. Kuehn, and J. Schmiidt, "Melt spinning preparation of bismuth telluride and partially alloying with IV-VI compounds for thermoelectric application," *Thermoelectr. power Gener.*, vol. 1044, pp. 115–120, 2008.

[81]   W. Xie, X. Tang, Y. Yan, Q. Zhang, and T. M. Tritt, "Unique nanostructures and enhanced thermoelectric performance of melt-spun BiSbTe alloys," *Appl. Phys. Lett.*, vol. 94, no. 10, 2009.

[82]   J. Schilz, M. Riffel, K. Pixius, and H. J. Meyer, "Synthesis of thermoelectric materials by mechanical alloying in planetary ball mills," in *Powder Technology*, 1999.

[83]   C. Suryanarayana, "Mechanical alloying and milling," *Progress in Materials Science*. 2001.

[84]   X. Z. Liao, J. Y. Huang, Y. T. Zhu, F. Zhou, and E. J. Lavernia, "Nanostructures and deformation mechanisms in a cryogenically ball-milled Al-Mg alloy," *Philos. Mag.*, vol. 83, no. 26, pp. 3065–3075, 2003.

[85]   Y. Lan, B. Poudel, Y. Ma, D. Wang, M. S. Dresselhaus, G. Chen, and Z. Ren,

"Structure study of bulk nanograined thermoelectric bismuth antimony telluride," *Nano Lett.*, vol. 9, no. 4, pp. 1419–1422, 2009.

[86]   H. Wang, J. F. Li, C. W. Nan, M. Zhou, W. Liu, B. P. Zhang, and T. Kita, "High-performance Ag0.8Pb18+xSbTe20 thermoelectric bulk materials fabricated by mechanical alloying and spark plasma sintering," *Appl. Phys. Lett.*, vol. 88, no. 9, pp. 20–23, 2006.

[87]   W. Xie, J. He, S. Zhu, T. Holgate, S. Wang, X. Tang, Q. Zhang, and T. M. Tritt, "Investigation of the sintering pressure and thermal conductivity anisotropy of melt-spun spark-plasma-sintered (Bi,Sb)2Te3 thermoelectric materials," *J. Mater. Res.*, vol. 26, no. 15, pp. 1791–1799, 2011.

[88]   M. Scheele, N. Oeschler, K. Meier, A. Kornowski, C. Klinke, and H. Weller, "Synthesis and thermoelectric characterization of Bi2Te 3 nanoparticles," *Adv. Funct. Mater.*, vol. 19, no. 21, pp. 3476–3483, 2009.

[89]   J. Yang, R. Chen, X. Fan, S. Bao, and W. Zhu, "Thermoelectric properties of silver-doped n-type Bi2Te 3-based material prepared by mechanical alloying and subsequent hot pressing," *J. Alloys Compd.*, vol. 407, no. 1–2, pp. 330–333, 2006.

[90]   P. Zou, G. Xu, and S. Wang, "Enhanced thermoelectric performance in n-type Bi2Te2.95Se0.05 bulks fabricated by high pressure sintering technique Ping," *Mater. Res. Bull.*, vol. 60, pp. 808–813, 2014.

[91]   A. Hilaal and R. Seeram, "Author's Accepted Manuscript A Review on the enhancement of Figure of Merit from Bulk to Nano Thermoelectric Materials," *Nano Energy*, pp. 1–39, 2012.

[92] F. Yu, B. Xu, J. Zhang, D. Yu, J. He, Z. Liu, and Y. Tian, "Structural and thermoelectric characterizations of high pressure sintered nanocrystalline Bi 2Te 3 bulks," *Mater. Res. Bull.*, vol. 47, no. 6, pp. 1432–1437, 2012.

[93] Z. Chen, M. Y. Lin, G. D. Xu, S. Chen, J. H. Zhang, and M. M. Wang, "Hydrothermal synthesized nanostructure Bi-Sb-Te thermoelectric materials," *J. Alloys Compd.*, vol. 588, pp. 384–387, 2014.

[94] M. Zhou, J. F. Li, and T. Kita, "Nanostructured AgPbmSbTem+2 system bulk materials with enhanced thermoelectric performance," *J. Am. Chem. Soc.*, vol. 130, no. 13, pp. 4527–4532, 2008.

[95] Z. H. Dughaish, "Lead telluride as a thermoelectric material for thermoelectric power generation," *Phys. B Condens. Matter*, vol. 322, no. 1–2, pp. 205–223, 2002.

[96] A. U. Khan, N. Vlachos, and T. Kyratsi, "High thermoelectric figure of merit of Mg2Si 0.55Sn0.4Ge0.05 materials doped with Bi and Sb," *Scr. Mater.*, vol. 69, no. 8, pp. 606–609, 2013.

[97] A. A. Usenko, D. O. Moskovskikh, M. V. Gorshenkov, A. V. Korotitskiy, S. D. Kaloshkin, A. I. Voronin, and V. V. Khovaylo, "Optimization of ball-milling process for preparation of Si-Ge nanostructured thermoelectric materials with a high figure of merit," *Scr. Mater.*, vol. 96, pp. 9–12, 2015.

[98] Z.-B. Xing, Z.-Y. Li, Q. Tan, T.-R. Wei, C.-F. Wu, and J.-F. Li, "Composition optimization of p-type AgSn m SbTe m+2 thermoelectric materials synthesized by mechanical alloying and spark plasma sintering," *J. Alloys Compd.*, vol. 615, pp.

451–455, 2014.

[99]   J. Rakovan, ": X-Ray Diffraction (XRD)," *Rocks Miner.*, vol. 79, pp. 351–353, 2004.

[100] J. Goldstein, D. Newbury, D. Joy, C. Lyman, P. Echlin, E. Lifshin, L. Sawyer, and J. Michael, *Scanning Electron Microscopy and X-ray Microanalysis*, vol. 1. 2003.

[101] S. Lazar, G. a Botton, M. Wu, F. D. Tichelaar, and H. W. Zandbergen, "High resolution EELS measurements on GaN in a m onochromated t ransmission e lectron m icroscope .," no. Figure 2, pp. 2–3, 2012.

[102] J. D. Menczel, H. E. Bair, M. Reading, L. Judovits, R. B. Prime, and S. Swier, "Differential Scanning Calorimetry (Dsc)," *Therm. Anal. Polym. Fundam. Appl.*, p. 688, 2009.

[103] M. Kisan, S. Sangathan, J. Nehru, and S. G. Pitroda, "Iso 6507-1:1," 2002.

[104] E. I. P. P. Panagiotidis, A. S. Antonatos, and G. M. Tsananas, "Case Depth Determination By Using Vickers Micro - Hardness Test Method At Trsc / Ppc Sa," *Hell. Soc. non distructive Test.*, no. October, pp. 11–14, 2007.

[105] E. S. Schwyter, T. Helbling, W. Glatz, and C. Hierold, "Fully automated measurement setup for non-destructive characterization of thermoelectric materials near room temperature.," *Rev. Sci. Instrum.*, vol. 83, no. 7, p. 074904, 2012.

[106] L. J. van der Pauw, "A method of measuring the resistivity and Hall coefficient on lamellae of arbitrary shape," *Philips Tech. Rev.*, vol. 20, pp. 220–224, 1958.

[107] T. Schneider, R. Allen, D. Koester, and S. Lee, "Thin Film Thermoelectric Power Generation: Enabling Waste Heat Recovery in High Heat Flux Environments," p.

25, 2007.

[108] S. A. Humphry-Baker and C. A. Schuh, "The nanocrystalline thermoelectric compound Bi2Te3 forms by a particle-wise explosive reaction during mechanical alloying," *Scr. Mater.*, vol. 65, no. 6, pp. 516–519, 2011.

[109] H. Li, H. Jing, Y. Han, G.-Q. Lu, and L. Xu, "Effects of mechanical alloying process and sintering methods on the microstructure and thermoelectric properties of bulk Bi 0.5 Sb 1.5 Te 3 alloy," *Intermetallics*, vol. 43, pp. 16–23, 2013.

[110] L.-D. Zhao, "Enhanced thermoelectric and mechanical properties in textured n-type Bi2Te3 prepared by spark plasma sintering," no. March 2016, 2008.

[111] S. Augustine and E. Mathai, "Dislocation, annealing and quenching effects on the microindentation hardness of Bi2Te3 and Bi2Te 2.9Se.1 single crystals," *Mater. Charact.*, vol. 52, no. 4–5, pp. 253–262, 2004.

[112] Y. Pan, T. R. Wei, Q. Cao, and J. F. Li, "Mechanically enhanced p- and n-type Bi2Te3-based thermoelectric materials reprocessed from commercial ingots by ball milling and spark plasma sintering," *Mater. Sci. Eng. B Solid-State Mater. Adv. Technol.*, 2015.

[113] J. Y. Yang, X. A. Fan, R. G. Chen, W. Zhu, S. Q. Bao, and X. K. Duan, "Consolidation and thermoelectric properties of n-type bismuth telluride based materials by mechanical alloying and hot pressing," *J. Alloys Compd.*, vol. 416, pp. 270–273, 2006.

[114] W. Kim, "Strategies for engineering phonon transport in thermoelectrics," *J. Mater. Chem. C*, vol. 3, pp. 10336–10348, 2015.

[115] G. Li, K. R. Gadelrab, T. Souier, P. L. Potapov, G. Chen, and M. Chiesa, "Mechanical properties of Bi $_x$ Sb $_{2-x}$ Te $_3$ nanostructured thermoelectric material," *Nanotechnology*, vol. 23, no. 6, p. 065703, 2012.

[116] F. A. Mohamed, "Correlation between the behavior of nanocrystalline HCP metals and the dislocation model for the minimum grain size obtainable by milling," *Mater. Sci. Eng. A*, vol. 527, no. 9, pp. 2157–2162, 2010.

[117] A. Mehdizadeh Dehkordi, M. Zebarjadi, J. He, and T. M. Tritt, "Thermoelectric power factor: Enhancement mechanisms and strategies for higher performance thermoelectric materials," *Materials Science and Engineering R: Reports*, vol. 97. pp. 1–22, 2015.